RL-TR-96-188
Final Technical Report
September 1996

60 AND 94 GHz WAVE-COUPLED ELECTRO-OPTIC MODULATORS

California Institute of Technology

William B. Bridges, Lee J. Burrows, Uri V. Cummings,
Reynold E. Johnson, and Finbar T. Sheehy

APPROVED FOR PUBLIC RELEASE; DISTRIBUTION UNLIMITED.

Rome Laboratory
Air Force Materiel Command
Rome, New York

This report has been reviewed by the Rome Laboratory Public Affairs Office (PA) and is releasable to the National Technical Information Service (NTIS). At NTIS it will be releasable to the general public, including foreign nations.

RL-TR-96-188 has been reviewed and is approved for publication.

APPROVED:

NORMAN P. BERNSTEIN
Project Engineer

FOR THE COMMANDER:

DONALD W. HANSON, Director
Surveillance & Photonics Directorate

If your address has changed or if you wish to be removed from the Rome Laboratory mailing list, or if the addressee is no longer employed by your organization, please notify RL/OCPC, 26 Electronic Pky, Rome, NY 13441-4514. This will assist us in maintaining a current mailing list.

Do not return copies of this report unless contractual obligations or notices on a specific document require that it be returned.

REPORT DOCUMENTATION PAGE

Form Approved
OMB No. 0704-0188

1. AGENCY USE ONLY *(Leave blank)*	2. REPORT DATE	3. REPORT TYPE AND DATES COVERED
		FINAL NOV 91 - NOV 94

4. TITLE AND SUBTITLE (A:ADMIN\sf298nb3.doc)

60 AND 94 GHZ WAVE-COUPLED ELECTRO-OPTIC MODULATORS

5. FUNDING NUMBERS

C - F30602-92-C-0005
PE - 63726F
PR - 2863
TA - 92
WU -47

6. AUTHOR(S)

WILLIAM B. BRIDGES, LEE J. BURROWS, URI V. CUMMINGS, REYNOLD E. JOHNSON, FINBAR T. SHEEHY

7. PERFORMING ORGANIZATION NAME(S) AND ADDRESS(ES)

CALIFORNIA INSTITUTE OF TECHNOLOGY
DIVISION OF ENGINEERING AND APPLIED SCIENCE
136-93
PASADENA, CA 91125

8. PERFORMING ORGANIZATION REPORT NUMBER

N/A

9. SPONSORING / MONITORING AGENCY NAME(S) AND ADDRESS(ES)

ROME LABORATORY/OCPC (AFMC)
25 ELECTRONIC PARKWAY
ROME NY 13441-4515

10. SPONSORING / MONITORING AGENCY REPORT NUMBER

RL-TR-96-188

11. SUPPLEMENTARY NOTES

ROME LABORATORY/OCPC PROJECT ENGINEER: NORMAN P. BERNSTEIN, (315)-330-3147

12a. DISTRIBUTION AVAILABILITY STATEMENT

APPROVED FOR PUBLIC RELEASE; DISTRIBUTION UNLIMITED

12b. DISTRIBUTION CODE

13. ABSTRACT *(Maximum 200 words)*

This report details the theory, fabrication, and testing of a method of wave-coupled RF energy into an optical modulator. The purpose of the effort was to investigate a method of improving the high frequency response of an electro-optical modulator through a novel optical and RF wave velocity matching technique. Theoretical studies indicated that the velocity matching technique was viable. Experimental results failed to confirm the theoretical studies but the source of the difficulties are now well understood. Most of these problems occurred in the fabrication of the masks for the modulators. Further efforts in this area are continuing.

14. SUBJECT TERMS

OPTICS, OPTICAL MODULATORS, ELECTROOPTICS, MILLIMETERWAVE, RF OPTICS.

15. NUMBER OF PAGES

96

16. PRICE CODE

17. SECURITY CLASSIFICATION OF REPORT	18. SECURITY CLASSIFICATION OF THIS PAGE	19. SECURITY CLASSIFICATION OF ABSTRACT	20. LIMITATION OF ABSTRACT
UNCLASSIFIED	**UNCLASSIFIED**	**UNCLASSIFIED**	**SAR**

NSN 7540-01-280-5500

Standard Form 298 (Rev. 2-89)
Prescribed by ANSI Std. Z39-18
298-102

INDEX

1.0 EXECUTIVE SUMMARY

This report documents the progress made in antenna-coupled lithium niobate electro-optic modulators for mm-waves over the three year period from November 1991 to November 1994. It also includes additional progress made following the end of the contract, through December 1995.

We have successfully demonstrated a mm-wave antenna-coupled modulator at 91 GHz based on an integrated optical waveguide directional coupler. This is the first such demonstration in the mm-wave region. While there are really no other mm-wave modulators with which to compare the sensitivity value of 0.196 m^2/Watt, it is not much lower than the values for conventional microwave modulators. It is better than the value of 0.072 m^2/Watt obtained at 91-98 GHz previously obtained by us with a bow-tie antenna-coupled Mach-Zehnder modulator. The directional coupler modulator exhibited excessive optical loss, but the source of the loss has been discovered and corrected. Additionally, improvements in the r-f transition from mm waveguide to the modulator have been made that should make a several-fold increase in the sensitivity.

The theory, design, and progress on a novel lithium niobate modulator that uses the modulator chip as a dielectric wave guide to couple to broad-band slot-V antennas is presented here. This novel modulator configuration has the promise of being an efficient, rugged device with broad-band capability in the mm-wave regions. Modulator chips have been fabricated for 20, 50 and 94 GHz and are now awaiting mounting and evaluation.

Research and development of proton-exchange waveguides at Caltech was undertaken, with the goal of fabricating our own modulators, rather than depending on the generosity of the Hughes Research Laboratories for our chips. We also hope to contribute to the solution of some problems that exist in annealed proton exchange guides currently being made by others in the industry. We present our view of the relevant physics in this report.

2.0 INTRODUCTION AND OUTLINE

2.1 INTRODUCTION

The work reported here was undertaken in the period November 1991 to November 1994. It was preceded by a one year contract in 1989-90 from Rome Laboratories. Even though the present contract has ended, the work on antenna-coupled modulators has continued, although at a much slower pace.

The concept of antenna-coupling to a segmented transmission overlaying optical waveguides in an electro-optic modulator was created to do phase-matching-on-the average and thus allow the effective length of the modulator to be greatly extended. While there is no lower bound in frequency to the use of this technique, it is not needed in modulators below about 1 GHz, since the modulator length there is limited by the available size of lithium niobate wafers, not phase mismatch. However, at mm wavelengths, it is crucial to have velocity matching for modulators longer than a few mm. And using a segmented transmission line with each section individually fed with its fraction of the input power, rather than one long transmission line with its attendant exponential attenuation, will also be required to reach wafer-limited lengths.

In the previous program we demonstrated the basic feasibility of the concept with phase modulators at 10 GHz and 60 GHz, and a broad-band intensity modulator at 91-98 GHz using a Mach-Zehnder modulator. In the present program we continued the demonstrations to include a 91 GHz narrow-band modulator using a directional coupler modulator. We also began the design and construction of a novel modulator arrangement that uses the modulator chip itself as a mm-wave dielectric waveguide, very broad-band antenna coupling (slot-V antennas) and the potential of a very rugged mechanical structure. We undertook a program to produce proton-exchange optical waveguides in lithium niobate at Caltech, and make measurements to contribute to the understanding of the processing and problems encountered

in modulators using such waveguides. We began the work necessary to fabricate modulator chips at Caltech, rather than depend on the informal cooperation with the Hughes Research Laboratories to obtain them.

Not all of our program goals were completed during the 3 year interval. We have continued the work at a reduced pace, and the progress and present status through December 1995 are included in this report.

2.2 OUTLINE

Section 3 reports the concept, design and status of the mm-wave directional coupler modulator. The evolution of this device work is quite interesting, in that a defect in the original waveguide masks was actually essential for the first successful demonstration of the device (but also contributed unacceptable optical loss). When the defect was discovered and corrected, it turned out that the modulator had to be redesigned to make it functional. The new modulator design has been fabricated and will be evaluated in 1996. **Section 4** reports our progress in improving the coupling from standard metal waveguide into the antenna arrays. **Section 5** and **Appendix A** present a summary of the theory of simple dipoles and V antennas on a dielectric interface. **Section 6** describes the concept and progress towards a demonstration of the novel Slot-V antenna-coupled modulator. **Section 7** reviews the physical processes involved in making optical waveguides in lithium niobate by a variety of methods. In particular, it introduces our view of the processes in proton exchange and annealed proton exchange lithium niobate waveguides, and their problems. Our progress in making and understanding annealed proton exchange waveguides is also presented. **Section 8** introduces the personnel that have contributed to this project, both directly, and as unpaid assistance. **Section 9** lists the meetings and conferences attended by project personnel, and the papers, publications, and patents related to the project. A **Glossary** of terms and abbreviations follows **Appendix A**.

3.0 DIRECTIONAL COUPLER MODULATORS

Early in this program (mid-1992) we undertook to design and fabricate a directional coupler modulator using the wave-coupled techniques that we had previously demonstrated with phase modulators and Mach-Zehnder modulators. The reasons were two-fold: First, it was not obvious to us initially that a directional coupler modulator (DCM) would work properly with the "phase-matching-on-the-average" offered by the wave-coupled approach. In a Mach-Zehnder modulator (MZM), the effect of not matching the phase velocities is simply understood, resulting in the familiar "sinc" functional variation with velocity mismatch. The effect of this velocity mismatch on a DCM is not so evident, and thus there was the possibility (in the absence of a complete analysis taking velocity mismatch into account) that a DCM would not work well at millimeter wavelengths using our techniques. The second reason we wished to demonstrate our techniques with DCM's was that DCM's appear currently to be the better candidates for linearized operation than dual MZM's, [Ref 3.1.] Since linearized, high dynamic range operation is likely to be important for any application using millimeter wave modulators, we felt it was important to see if wave-coupling was applicable to DCM's.

3.1 THEORY OF THE DIRECTIONAL COUPLER MODULATOR

The basic principle of a DCM is illustrated in Fig. 3.1. Two integrated optical waveguides are arranged to run parallel and very close to one another for some distance L. If the two guides are sufficiently close so that the exponentially-decaying (evanescent) fields outside the core region of one guide overlap the evanescent fields of the other guide, then some power in the first guide will be transferred to the second guide, exciting the normal propagating mode of that guide. (We assume here that both waveguides are dimensioned such that only the lowest-order mode propagates in each guide.) Thus, if we launch all of the optical input power into one guide, a certain fraction of that input will appear in the second guide in the distance L. The size of the fraction is determined by

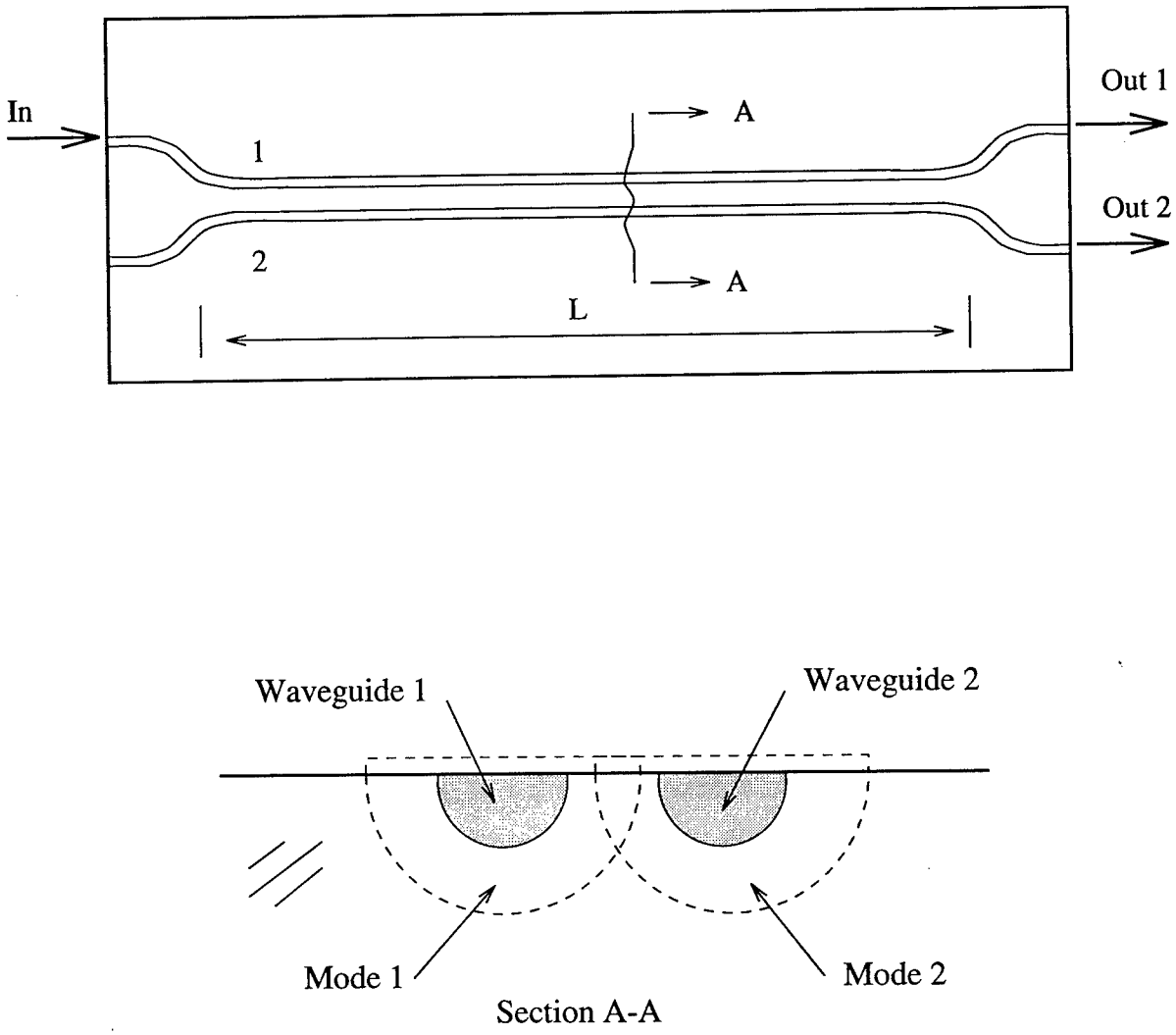

Fig. 3.1 Schematic representation of integrated optical waveguide directional coupler.

how close the two guides are with respect to one another physically, the exponential decay rates of the modes in the two guides, and the propagation constants in the two guides. (For a detailed theory of directional couplers see Refs. 3.2 or 3.3, for example.) It turns out that if the two guides have identical propagation constants β, then all of the power in the first guide can be transferred to the second in some distance L_o, termed the transfer distance.

By the symmetry of the two guides it is easy to see that if all the power is now in the second guide and the overall length of the coupler is greater than L_o, then the power will begin to transfer back to the first guide, and after a total distance $2L_o$, the power will all be returned to the first guide. And so on, if the length is longer still. The power "beats" back and forth between the two guides with a spatial period $2L_o$, as shown in Fig 3.2. Thus by choosing the overall length correctly, any given split of power between the two output ports can be obtained.

If the two optical waveguides are not identical in propagation constant β, but rather have constants β_1 and β_2 which differ by $\Delta\beta=\beta_1-\beta_2$, then all of the power cannot be transferred, although a fraction of the power will still beat back and forth between the two waveguides, also shown in Fig. 3.2. The larger $\Delta\beta$, the smaller the fraction that can be transferred.

To make an electro-optic modulator out of the directional coupler of Fig. 3.1, we need to fabricate the optical waveguides in an electro-optical material such as lithium niobate, and apply electrodes in the vicinity of the two waveguides as illustrated in Fig. 3.3 so that the β's in the two waveguides can be changed by applying a voltage to the two electrodes. For example, if the two guides are physically identical, then they will have equal β's . We next choose the overall length L to be one transfer length, L_s. If we arrange the electrodes as shown in Fig 3.3, then the voltage applied to the electrodes will produce equal and opposite electric fields in the vicinity of the two guides which will result in equal and opposite changes in the β's of the waveguides. This will spoil the complete transfer, causing some of the power to reappear in the original guide. If the voltage is increased, this electro-optically-induced $\Delta\beta$ will cause the power in the first guide to increase, eventually causing *all* of the power to re-appear in the first guide. The value of the voltage that

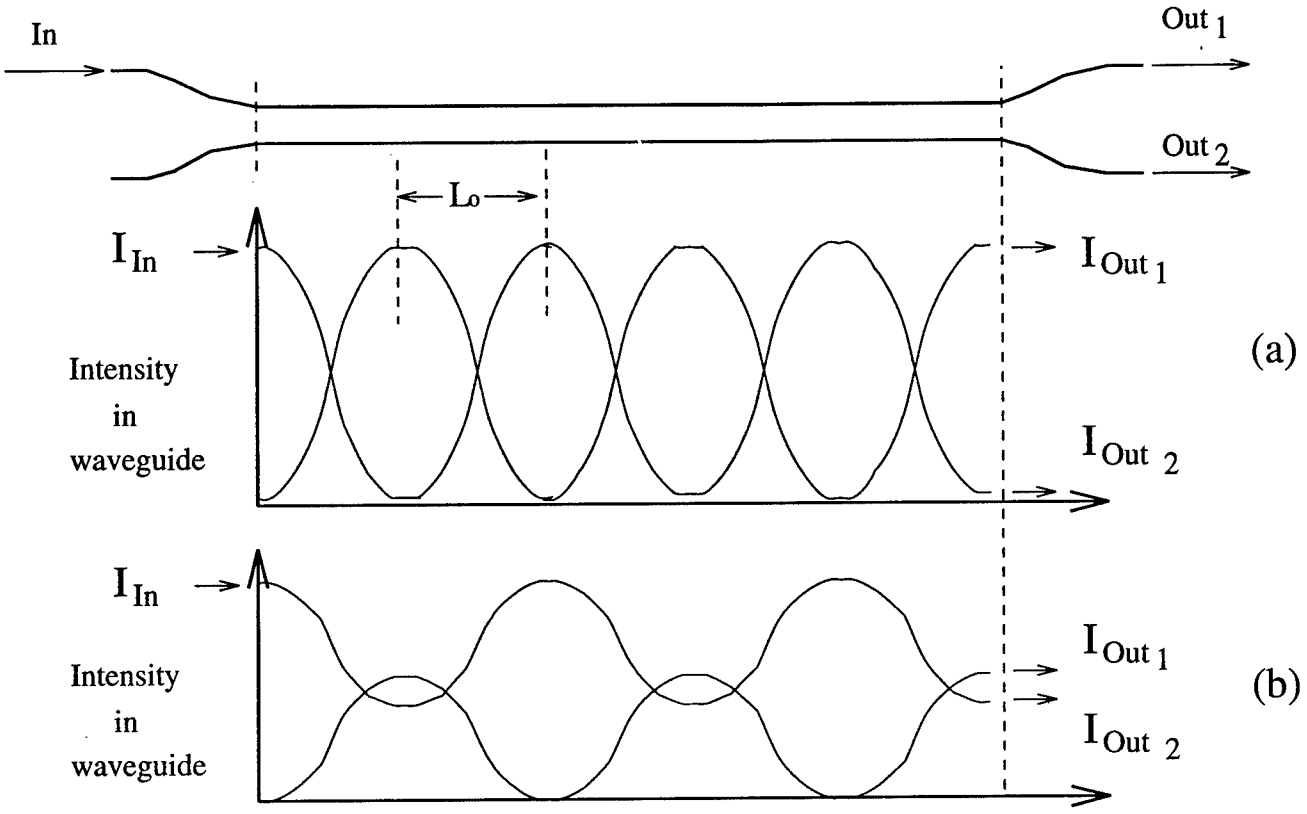

Fig. 3.2 Spatial transfer of optical excitation in a directional coupler for (a) identical optical waveguides, $\Delta\beta=0$, and (b) non-identical waveguides, $\Delta\beta\neq0$.

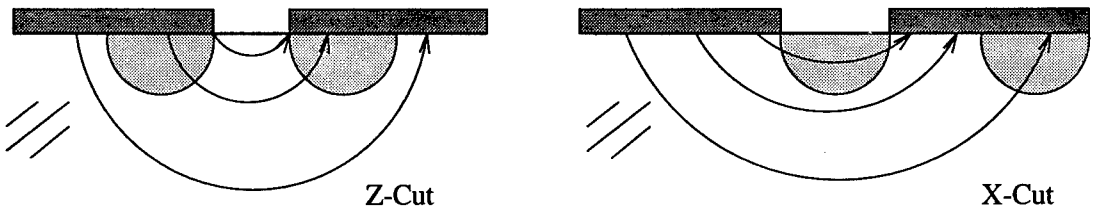

Fig. 3.3 End view of directional coupler modulator showing electrode positioning for both z-cut and x-cut modulators. The z-cut orientation is used in the DCM's fabricated under this contract.

causes this is termed the transfer voltage, V_s. If the voltage is increased further, some of the power is transferred back to the second guide, but complete transfer cannot be obtained, since there is now a sufficiently large $\Delta\beta$ to prevent it. The resulting curve of power in the first guide versus applied voltage is shown in Fig. 3.4. Note that the curve is symmetrical about zero volts; the sign of the electro-optically-induced $\Delta\beta$ does not make a difference in "spoiling" the complete transfer. (The equations used to produce this curve are given in Sec. 3.3.)

To achieve reasonably linear operation, a dc bias point is usually chosen to pick out the most linear portion of the transfer function shown in Fig. 3.4. This point is about 0.43 V_s for a normal DCM. This is analogous to biasing a MZM at 0.50 V_π. (Other bias points can be employed for special purposes, for example, to minimize third-order intermodulation at the expense of increased second harmonic content, as described in Ref. 3.1) The desired modulation is then added to this bias voltage.

3.2 WAVE-COUPLED 94 GHZ DCM DESIGN FTS-1

The first design for a wave-coupled directional-coupler modulator was made by Caltech graduate student F. T. Sheehy. The design frequency was chosen as 94 GHz, and resonant antenna-plus-transmission line segments were chosen instead of the broad-band "bow-tie" antennas used in the 94 GHz Mach-Zehnder experiment (Ref. 3.4). The reason for this choice was that the resonant fields on the transmission line segments were expected to be stronger than those on the better-matched bow-tie design, and we wished to have the strongest interaction possible for this initial DCM experiment. The design chosen was the two-half-waves-in-phase antenna, coupled to an open-circuited transmission line. The lengths of the "half-waves" were modified according to the "fat" antenna theory (see Ref. 3.5, for example), and thus were about 0.33 λ_g, where λ_g is the wavelength corrected for the effective refractive index of a transmission line on the surface of lithium niobate, $n_{eff} = 3.8$ (which was also confirmed by experiment in Ref. 3.5).

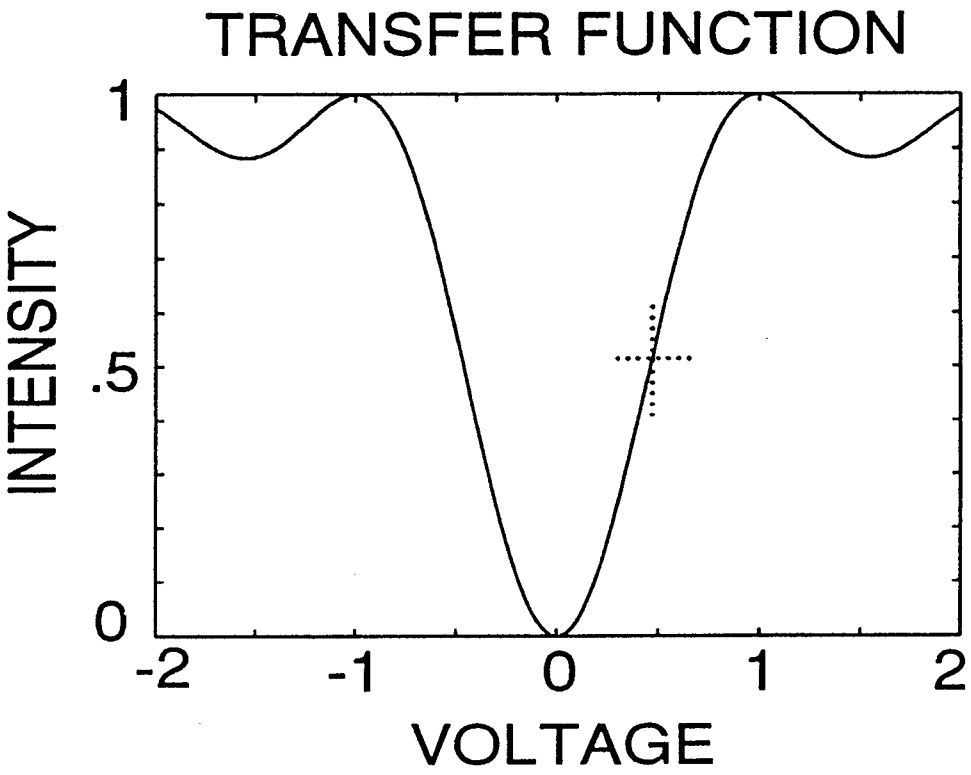

Fig. 3.4 Transfer function for a simple directional coupler modulator one transfer length (L_0) long and with transfer voltage V_s.

The choice of the resonant dipole-plus-transmission-line structure has an unfortunate consequence, however: There is no "cold" portion of the antenna near the ends where d-c bias lines can be connected conveniently. We had previously used this structure only in phase modulators, which require no d-c bias voltage. In the 94 GHz Mach-Zehnder with the bow-tie antennas, we were able to attach the bias lines onto the end of the antenna elements, since (according to commonly accepted theory) the ends of the bow-tie are "cold" to r-f . Another method of biasing the directional coupler operating point to the linear portion of the transfer curve was employed instead. D-c electrodes were added to the same directional coupler, outside the region covered by antenna-coupled region, to shift the ordinary DCM transfer function so that the linear portion of the transfer function for the antenna-coupled region occurs at zero bias voltage, as shown in Fig. 3.5. The design actually used had a *pair* of d-c bias electrodes on either side of the antenna-coupled region., for possible future "linearization" of the kind described in Ref. 3.1.

Figure 3.6 shows the actual mask used. Twelve DCM's were fabricated at the same time, with six having the same electrode lengths, and six having different electrode lengths. This particular mix of modulator samples resulted from designing our electrodes to fit a pre-existing directional coupler mask (LINC-1) designed for other modulators by J. H. Schaffner at Hughes Research Labs (HRL). The antennas had overall lengths of 0.478 mm, and the transmission line segments were 0.42 mm long in all cases. The optical waveguides were fabricated using a standard formula of titanium in-diffusion to produce single mode guides at 1.3 μm wavelength that had been worked out at HRL. The electrodes were evaporated gold (1000 Å) over a thin layer of SiO_2 (3400 Å).

Measurements on these modulators were begun at Caltech early in 1993. The optical performance was particularly poor, with optical losses of just under 20 dB. And the expected transfer functions of the d-c bias electrodes was not realized. To make sense of the d-c transfer function, the antenna-coupled regions were shorted together with silver paint. This proved futile, and also had the unfortunate side effect of shorting out all the electrodes completely. This particular modulator sample was abandoned to concentrate on other tasks necessary to F. T. Sheehy's Ph. D. dissertation, so that he would complete it in time for graduation in June, 1993. Only the design was given in his dissertation (Ref. 3.6).

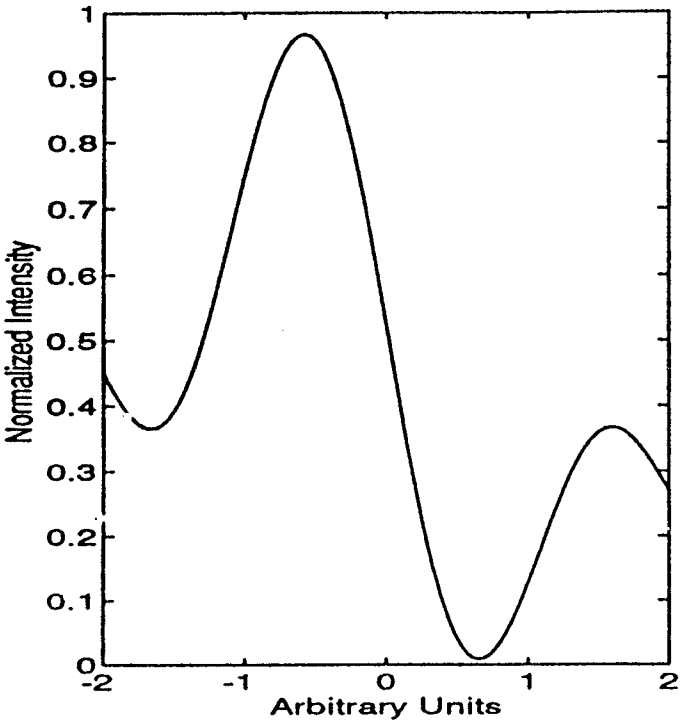

Fig. 3.5 Theoretical transfer function of the antenna-coupled region of the FTS-1 DCM design when the correct bias voltages are applied to the two auxiliary bias sections.

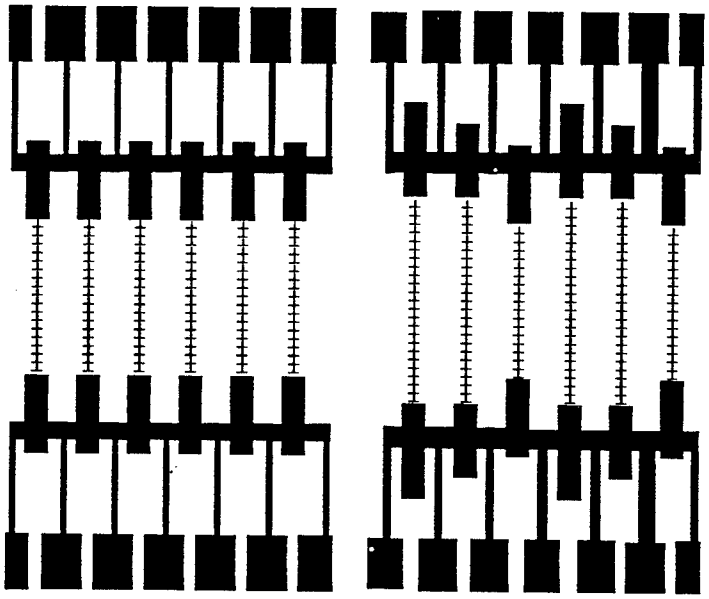

Fig. 3.6 Actual electrode mask used in FTS-1 design, to make 12 modulators on a 3" diameter $LiNbO_3$ wafer. The gaps between electrode pairs do not show at this scale. The particular modulator used in the transfer function measurements is the fourth from the top.

3.3 SUCCESSFUL OPERATION OF THE FTS-1 DCM

An opportunity to re-address the FTS-1 antenna-coupled DCM arose in June 1993, when Uri V. Cummings joined our research group as a Summer Undergraduate Research Fellow (SURF). Trying to understand Sheehy's DCM design seemed to be a good project. We began by undertaking somewhat more heroic measures in cleaning the silver particles out of the gold electrode structures, including some acid etches, ultrasonic agitation, and (finally) "zapping" with applied voltage to vaporize the remaining particles. A few of the modulator d-c electrodes were thus un-shorted.

The d-c transfer functions measured on these unshorted bias electrodes, initially exhibited the same puzzling results Sheehy had noted. However, careful measurement produced some curves that began to resemble transfer functions, but with the zero voltage scale unexpectedly shifted. An example is shown in Fig. 3.7, with the originally-expected transfer function included for comparison. The equations for the output intensities of a simple directional coupler are included in Fig. 3.7. The transfer function of a DCM with identical optical waveguides ($\Delta\beta=0$) should be symmetrical around zero applied voltage, since the equations contain only $(\Delta\beta)^2$, and thus the transmission should be independent of the sign of the electro-optic $\Delta\beta$. However, if the optical directional coupler has a built-in asymmetry in the β's for the two optical waveguides, then there would be a *static* value of $\Delta\beta_s$ as well as an electo-optic $\Delta\beta_e$, and these two combine in a sign-sensitive fashion, $(\Delta\beta_e+\Delta\beta_s)^2$, resulting in an asymmetric curve around zero applied voltage. After a series of careful measurements and some curve fitting, we determined this must be the case. Figure 3.8 shows a final fit between theory and experiment for the transfer function of one of the FTS-1 modulator d-c bias electrodes. Figure 3.8a shows the fit using all of the data points taken, while Fig. 3.8b shows a better fit for the lower voltage regions when the data points at higher voltages are omitted. This latter fit seems more appropriate, since the transmission values at higher applied voltages were not stable with time. At the time we took the data in Fig. 3.8, we did not know the physical origin of $\Delta\beta_s$, but we had determined its value of 1.7 radians/cm by curve fitting.

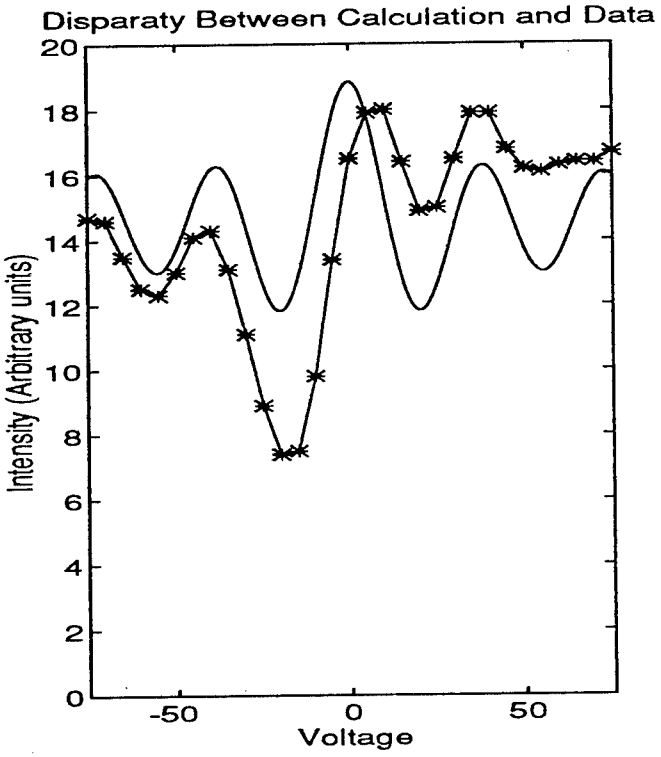

$$I_{out} = \frac{I_0}{1 + (\frac{\Delta\beta_s + \Delta\beta_e}{\kappa})^2} \sin^2(\theta \sqrt{1 + (\frac{\Delta\beta_s + \Delta\beta_e}{\kappa})^2})$$

Fig. 3.7 Transfer function and equations for the d-c bias section of the FTS-1 DCM with a built-in static $\Delta\beta_s$.

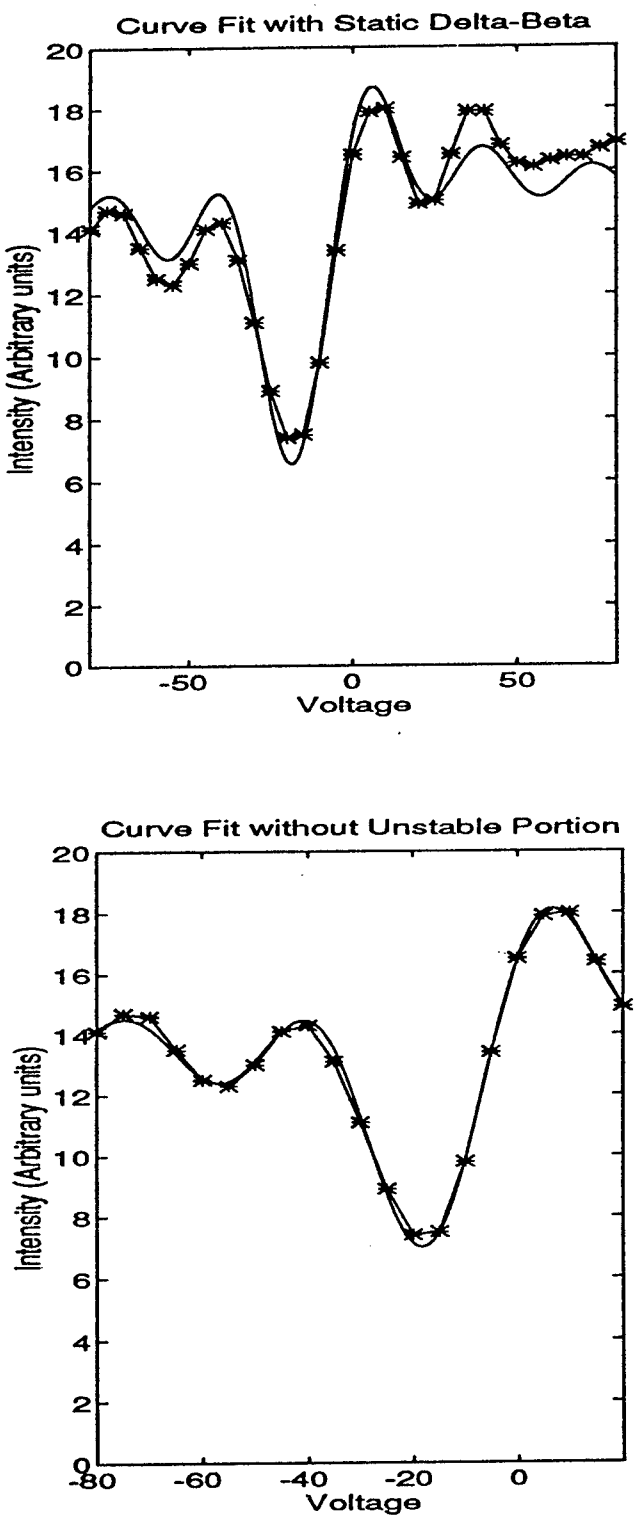

Fig. 3.8 Final experimental fit to theory for d-c bias region of FTS-1 design. The value of $\Delta\beta_s$ required was 1.7 rad/m.

Armed with this insight, we were able to determine the voltages to apply to the d-c bias electrodes to shift the transfer function for the antenna-coupled region so that it would have its linear portion centered at zero voltage. The same mm-wave set up used by Sheehy in the 94 GHz M-Z experiment (Ref. 3.5) was reassembled and applied to the DCM. This set up is shown schematically in Fig 3.9. This time a 5 mW, 1.3 μm Nd-YAG laser was available for the measurements. The same 94 GHz Varian klystron oscillator used (now producing a maximum of only 35 mW). The output from the WR-10 waveguide was coupled to a 1 mm thick polypropylene slab waveguide, tapered from a point inserted in the 4 mm width of the WR-10 waveguide up to 20 mm width of the antenna array. This slab was matched to a 1 mm thick, 20 mm wide wedge of lithium niobate slab guide through a thin (roughly $\lambda_g/4$) piece of ε=9 Stycast dielectric, acting as a matching layer. The wedge-shaped lithium niobate slab guide was glued to the bottom side of the modulator chip so that the 1 mm x 20 mm end of that guide illuminated the array of antennas. As in previous experiments, the modulation was detected by passing the modulated light through a scanning Fabry-Perot interferometer, and measuring the amplitude of the modulation sidebands relative to the carrier amplitude. The percentage modulation can then be determined from this ratio.

For the one sample of twelve on the chip that had unshorted electrodes, we obtained a value of optical modulation index (squared) per unit of modulation power of 0.196 [m^2/W] at 91 GHz (the klystron frequency that gave the highest output power). The quantity "m" is the dimension-less modulation index. This value was actually better than the value obtained by Sheehy on the bow-tie MZ modulator, 0.072 [m^2/W]. These results were reported at the PSAA-IV meeting in January 1994 [Ref. 3.7]. However, before writing up the results for publication, we thought it would be wise to make another sample, one with better optical transmission that would give a better signal-to-noise ratio in the measurements. A new modulator chip using the same HRL designed directional coupler waveguide mask (LINC-1) and the same FTS-1 electrode mask was fabricated at HRL.

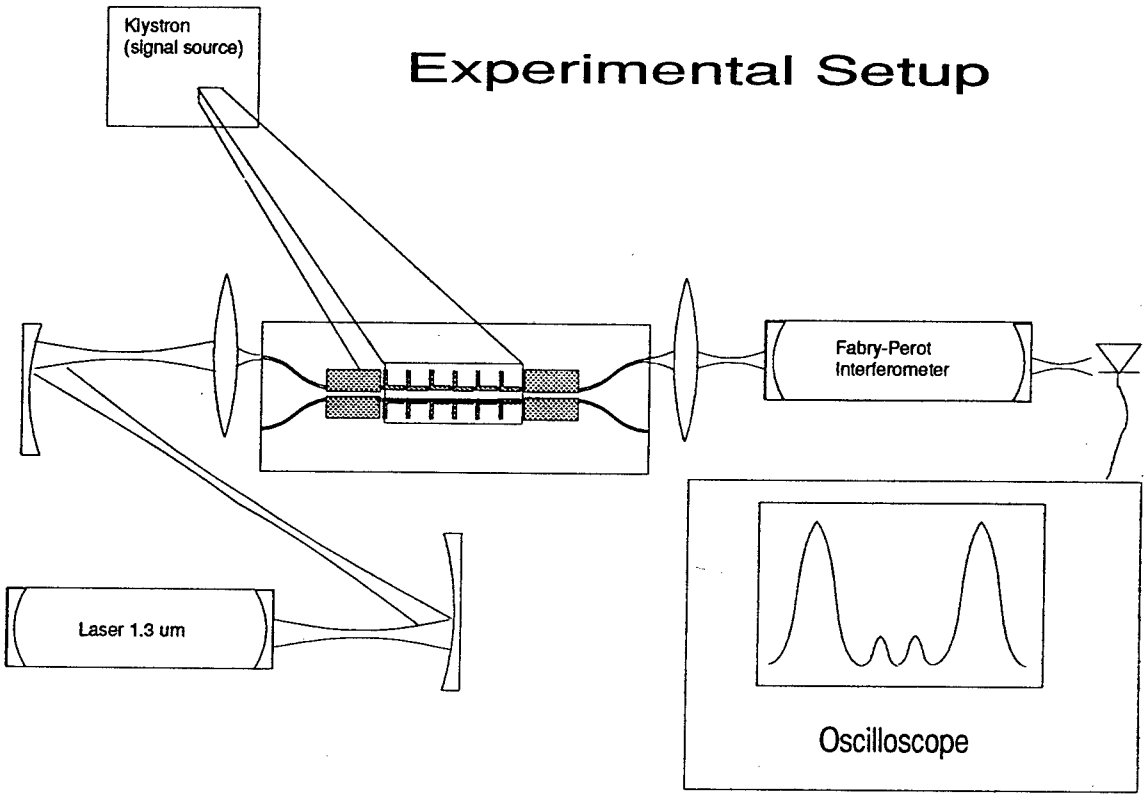

Fig. 3.9 Measurement set-up for FTS-1 DCM evaluation.

3.4 PHYSICAL ORIGIN OF THE STATIC $\Delta\beta_s$

While this modulator chip was being fabricated, we undertook to make both positive and negative copies of all the masks being used in this program so that we could begin to fabricate our own modulators at Caltech using Prof. Axel Scherer's photolithographic facilities. While checking the quality of the mask copies under a microscope, we discovered that the HRL-designed LINC-1 directional coupler waveguide mask had serious defects in it. The defects consisted of missing pieces of the chromium mask material, just at the waveguide edges. These pieces were of the order of a few to ten microns along the direction of the guide and a few to ten microns transverse to the guide. Align-Rite, the company that fabricates the masks for HRL and Caltech, refers to such defects as "mouse-bite" defects, since they resemble a tiny "bite" taken out of the edge of the metal mask. Such a defect is shown schematically in Fig. 3.10. We initially thought that such defects were due to rough handling of the mask, but recently (Fall, 1995), HRL has had new masks fabricated by Align-Rite which also exhibit "mouse-bite" defects. Several discussions with Align-Rite have not completely resolved the origin of these defects, but the current thinking is that small electro-static discharges from the lithium niobate substrate to the mask during the near-contact used in exposing the mask can "knock off" edges of the mask. Steps currently being taken at HRL include plating the back side of the lithium niobate substrate with a thin titanium layer prior to the contact exposure to reduce the thermally generated electro-static charges on the surface. It remains to be seen whether or not this will eliminate "mouse bites."

However, once the "mouse bites" were discovered on the original HRL LINC-1 waveguide mask, we examined the original FTS-1 modulator chips and found that the "mouse bites" were *faithfully reproduced on its waveguides!* This, then, is the physical origin of both the static $\Delta\beta_s$ and the high optical loss observed in the waveguides. At a "mouse bite", the guide is perhaps twice as wide for a distance of ten microns or so, causing a change in the local β in that guide, and causing the guided wave to spread so that not all of it is intercepted by the normal waveguide on the other side of the "mouse bite." Unfortunately, the new samples of the FTS-1 modulator chips fabricated at HRL had already been fabricated with the same defective mask, so they were as flawed as the original chip.

a

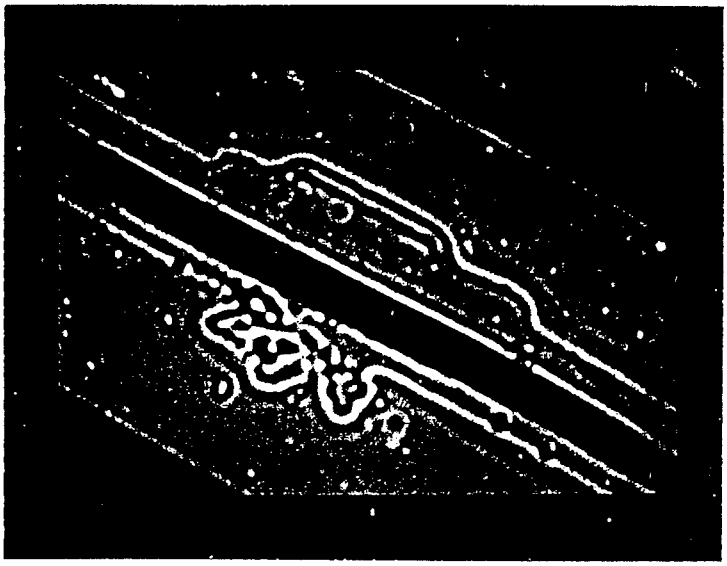

b

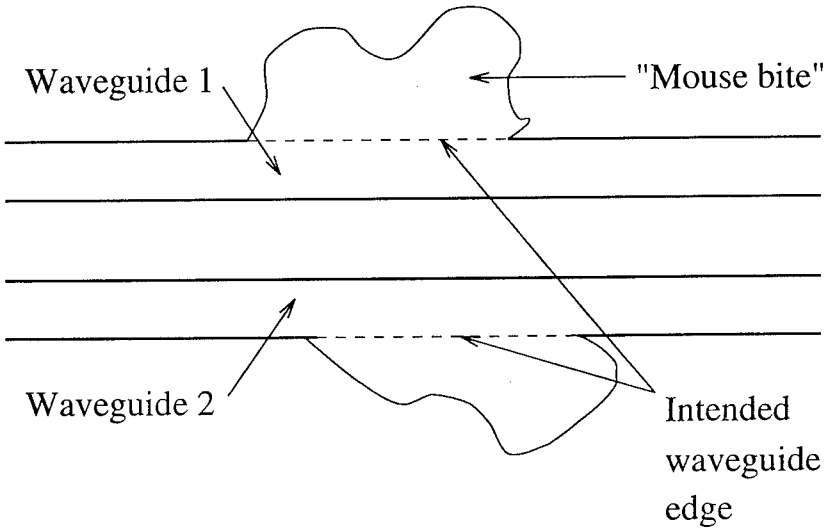

Fig. 3.10 "Mouse-bite" defects (a) on LINC-1 waveguide mask , and (b) schematic representation.

A new waveguide mask, identical to the original LINC-1 so that it would fit the FTS-1 electrode mask, was ordered from Align-Rite. This was received in mid 1994 and used successfully (without developing "mouse bites", even though we were not aware of the electrostatic discharge hypothesis and had taken no precautions to avoid them) to make a new set of FTS-1 modulators. Measurements at Caltech showed two major differences from the original FTS-1 modulators: (1) The new samples had good optical transmission, the order of 8 dB insertion loss at 1.3 μm, and (2) the transfer function of the dc bias electrodes was completely different, notably, there was very little change in transmission with the same applied voltage. While (1) was very encouraging, and indicates that the "mouse bites" were indeed the probable source of the high optical loss, (2) was upsetting indeed. The calculated transfer function for a dc bias electrode with $\Delta\beta_s = 0$ was already shown in Fig 3.7, and this is what we expected to see. An explanation for this unexpected behavior was (fortuitously) discovered about the same time as it was observed. On a completely different project, Dr. Cel Gaeta at HRL was remeasuring the coupling coefficients in directional couplers samples as a function of the waveguide dimensions and separations, and concluded that his original design data overstated the value of the coupling coefficient for the dimensions and separations used in the LINC-1 HRL mask design, the one used also in all the FTS-1 modulators. We used Gaeta's new curves to analyze the FTS-1 design and concluded that the dc bias sections were, indeed, too short to have much effect; what we observed in the lab was, unfortunately, just what we should have seen. We are forced to conclude that the only reason the original FTS-1 modulator worked in the first place was that the "mouse bites" introduced sufficient static $\Delta\beta_s$ to bias the modulator to a region where an additional electrical dc bias would just put the antenna transfer curve with a slope at zero bias. Had there been no "mouse bites," the bias electrodes would never have allowed us to make it work! Of course, the "mouse bites" also had the undesired effect of introducing unacceptable optical loss.

3.5 PROGRESS SINCE THE END OF THE CONTRACT

The situation described above was extant in November 1994, when the present contract ended. However, since then we have continued, albeit slowly, to pursue this ill-starred (but still promising) modulator. Using Gaeta's new coupling coefficients, we have designed a new waveguide mask (UVC-wg-1) and a new electrode mask for it (UVC-el-1) that should work as originally intended by Sheehy. The dc electrodes are relatively longer and the waveguides are closer together. These masks appear in Fig. 3.11. The new waveguide mask contains Mach-Zehnder waveguides and straight waveguides, as well as directional couplers, allowing it to be used for future projects. as well. Modulator samples will be fabricated at HRL using these masks as soon as they are received from Align-Rite, and then evaluated at Caltech, early in 1996. (We are moving to a new building early in December, and should have the laboratory up and running early in January 1996.)

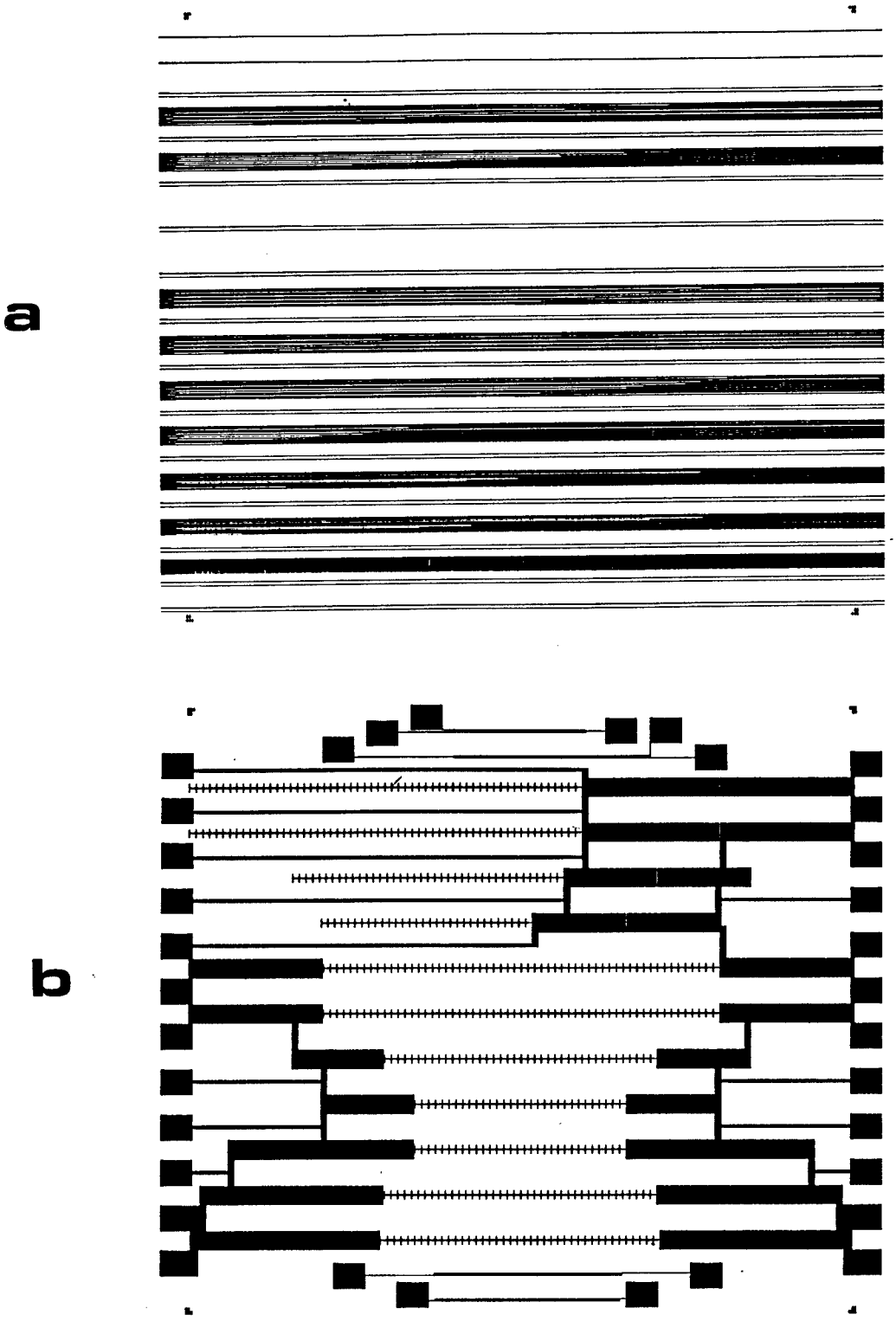

Fig. 3.11 (a) Waveguide mask UVC-wg-1 and (b) electrode mask UVC-el-1 for redesigned antenna-coupled DCM similar to FTS-1.

3.6 DIRECTIONAL COUPLER MODULATOR REFRENCES

3.1 W. B. Bridges and J. H. Schaffner, " Distortion in Linearized Electrooptic Modulators." invited paper in joint issues of IEEE Trans. on Microwave Theory and Techniques, vol. 43, pp. 2184-2197, and J. Lightwave Technology, September 1994.

3.2 E. A. J. Marcatili, "Dielectric Rectangular Waveguide and Directional Coupler for Integrated Optics," Bell Sys. Tech. J., vol.48, pp. 2017-2132, September 1969.

3.3 W. H. Louisell, *Coupled Mode and Parametric Electronics,* Wiley, 1960, Chapter 5.

3.4 F. T. Sheehy, W. B. Bridges, and J. H. Schaffner, "60 GHz and 94 GHz Antenna-Coupled $LiNbO_3$ Electrooptic Modulators," IEEE Phot. Tech. Lett., vol. 5, pp. 307-310, March 1993.

3.5 R. C. Johnson and H. Jasik, *Antenna Engineering Handbook, 2nd Edition,* McGraw-Hill, 1984, Chapter 4 by C. T. Tai, Figs., 4.3, 4.7.

3.6 F. T. Sheehy, "Antenna-Coupled mm-Wave Electro-Optic Modulators and Linearized Electro-Optic Modulators," Ph. D. dissertation, California Institute of Technology, June 1993.

3.7 W. B. Bridges, U. V. Cummings, F. T. Sheehy, and J. H. Schaffner, "Wave-Coupled $LiNbO_3$ Directional Coupler Modulator at 94 GHz," Paper 4.3, Photonic Systems for Antenna Applications-IV, Monterey CA, 18-21 January 1994.

4.0 R-F COUPLING IMPROVEMENT

4.1 INTRODUCTION

Having demonstrated the basic idea of wave-coupling and velocity-matching "on the average", we wish to improve the overall modulator performance. One important facet of this improvement is to maximize the coupling of the r-f input power into the antenna array. We have approached this task in two ways:

(1) Experiments at 94 GHz of back-to-back dielectric feeds. These experiments do not address the feed-to-antenna coupling portion nor the antenna type, but they do allow for improvements in the metal waveguide-to-tapered slab dielectric waveguide transition, and the coupling from low to high dielectric constant slabs.

(2) The development of a model test range at 10 GHz to try out different ideas in coupling improvement. The entire arrangement of waveguide, transition, and antenna type can be modeled, and the actual transmission efficiency from the metal waveguide feed to the antenna terminals on the modulator substrate determined. The range allows for easy modification of antennas.

4.2 TRANSITION DESIGN THEORY

The trick to increasing the efficiency of our mm-wave modulators lies in improving the coupling from the source wave guide into the antenna array. Ultimately, this is an antenna problem. However, first we must couple the power out of the source waveguide into an appropriate dielectric waveguide with a cross section that matches the antenna, and a phase distribution that is uniform across the array.

The first step, that of coupling radiation out of a standard rectangular waveguide into a slab dielectric waveguide by means of a tapered section positioned in an open-ended horn, is

actually easily done and turns out to be quite efficient, as long as the dielectric constant of the slab waveguide is not too high (i.e. $\varepsilon \sim 2$) nor the taper too abrupt. The taper is used to broaden the slab waveguide so that its width matches the length of the antenna array on the modulator substrate. Next, we must make a transition into a material with the same dielectric constant as lithium niobate (28 or 41, depending on the modulator crystal axis orientation used.) We need to do this with as little reflection as possible. In the past we have used one or more "quarter-wave" dielectric slab waveguide matching sections of an intermediate dielectric constant to make this transition. However, there are some problems in designing "quarter-wave" sections in dielectric waveguides that don't occur in metal waveguides, and these are discussed below. Finally, the high-dielectric constant slab guide is attached to the modulator. Here, the mode of the slab guide must match some desired *near-field distribution* of the antennas in the array; this is what we meant by the coupling being ultimately an antenna problem. In the discussion given below, we ignore this problem, and concentrate on the first two transitions: into the low-dielectric constant guide and the low-to-high dielectric constant transition

Before beginning the discussion, we should point out that the field theory for dielectric waveguides is not nearly so well developed as the field theory for closed metal waveguides. For example, no closed-form theory exists for simple uniform rectangular dielectric waveguides; only approximate theories with numerical results exist. Perhaps the best known of the approximate theories is that of Marcatili [Ref. 4.[1]], which gives us some insight, but has limitations in doing actual designs. And no theory exists for non-uniform guides, e.g. tapers. Nor is there a reasonable theory for discontinuities. (There are a wealth of calculations for discontinuities in closed metal waveguides, and even though they are all numerical, they at least provide design data.) So the best we can do is patch together pictures of what we do know from the two closed-form solutions that exist (the infinitely-broad dielectric slab guide and the circular cross-section guide) to give us a picture of the situations we actually have.

Visualizing the transition from standard rectangular metal waveguide to a slab dielectric guide via a one-dimensional taper fits the above procedure reasonably well. We know the field

distributions in the TE_{10} mode of standard metal wave guide. We also know the exact field distribution of the TM_1 mode of a dielectric slab of infinite width. The TM_1 mode has the right polarization to match the polarization of the antennas. However, the slab we use also has a finite width as well as thickness. We could appeal to Marcatili, who would name the desired mode "E_{11}^{y}", assuming the y-direction is normal to the slab surface. But even Marcatili's theory doesn't give us a complete mathematical description of the modal fields. And, of course, we are on our own for the tapered section. However, combined with what we know from the only other closed form solution, that of a cylindrical dielectric waveguide, we can "guess" the field distributions fairly well..

The trick is to distort the fields from the source mode to the desired mode without introducing reflections or, since dielectric waveguides are "open" structures, without introducing *radiation*. And experimentally we have done this pretty well, provided, as we said in the introduction, "the dielectric constant of the slab waveguide is not too high nor the taper too abrupt." In standard metal waveguides, "not too abrupt" usually means a smooth taper of 10 to 20 % in cross section per guide wavelength [Ref. 4.2]. Experimentally we have found a somewhat different result: If the dielectric constant of the tapered section is 2.5 (polypropylene or polystyrene) very good coupling is obtained with a wide variety of tapers. But if the tapered section is lithium niobate, with a dielectric constant of 28 or 42, depending on the orientation, *no coupling is obtained with any taper, no matter how gradual!*

This result did not come as a complete surprise. It is consistent with experiments at Caltech in the late 1970's on another program in which we had to couple from a rectangular metal waveguide to a cylindrical rod. A sequence of tapered rods were made of Stycast® with dielectric constants of 3, 4, 5, 10, 20, 30, and 32. Excellent coupling was obtained for values less than 10 with even short tapers (or even no taper at all), and *no* coupling was obtained for the higher three values, no matter how shallow the taper! We do not understand the reason for this rather abrupt change in behavior at a particular dielectric constant; it would be a good subject for future theoretical study on another program.

However, in this earlier program, we were able to couple into the high dielectric constant guide by first coupling into a guide of lower dielectric constant, then using a "quarter-wave" section of intermediate dielectric constant to couple to the higher dielectric constant guide. Thus, we were able to couple into rods of permittivity 20, 30 and 32 with some reasonable efficiency. The problem here is knowing how to design the "quarter-wave" section. The length of the section must be a quarter of a guide wavelength long (or an odd multiple thereof), and this can be calculated for round rods and infinite slab waveguides. We could also use Marcatili's approximate theory to find the guide wavelength in a rectangular guide, but our guides are sufficiently broad following a low dielectric constant taper, that the infinite slab calculation is likely good enough.

An even bigger problem than the guide wavelength is the radiation that occurs at the discontinuities at the ends of the quarter-wave section. Even if all three slab waveguides are the same height, there is a mismatch in the geometric distribution of the modes in the three sections: The mode will be most tightly confined in the highest dielectric constant region, and least tightly confined in the low dielectric constant region. The evanescent "tails" of the modes in the regions outside the dielectric will not match, and consequently, there will be both reflection and radiation at the junctions. There will also be small differences in the transverse distribution of fields inside the slabs as well. Making the slab thickness different in the three guides does not solve the problem; in fact, it will likely make the reflection and radiation worse. To compound the problem, some of the radiation at the input to the quarter-wave section can couple back into the guide at the other end (where the discontinuity acts as a receiving antenna) after having made the trip in air, rather than the intermediate dielectric, so that the effective length is no longer a quarter-wave. Very little theory has been attempted even on a single discontinuity, much less two in series. Such problems do not occur in quarter-wave sections in closed metal waveguides, where the mode distributions automatically match.

Despite the problems with the theory, we had used quarter-wave matching sections in all our experiments, with reasonable success. Thus we undertook an optimization of the configuration by trial and error.

4.3 EXPERIMENTS AT 94 GHZ

To make a qualitative measurement of the transition efficiency at 94 GHz, we set up two such transitions "back-to-back". That is, we set up a standard W-band horn (fed by WR-10 waveguide) as a radiation, used a tapered polypropylene slab waveguide 1 mm thick with its point positioned in the throat of the horn, followed by a "quarter- wave" section, then a section of lithium niobate 1 mm thick, and about 10 mm long, then another "quarter-wave", and another polypropylene taper into a second W-band horn. Thus, the setup is symmetrical about the center of the lithium niobate section. The width of the lithium niobate section and the two quarter-wave sections was about 20 mm, the typical length of our modulators.

The input power was monitored by a directional coupler and crystal detector, and the output power was measured by a second crystal detector. The reference of 0 dB was measured by noting the two detector readings when the horn-to-horn section was removed, and the WR-10 flanges were connected.

The degrees of freedom in this set up are thus, the angle of the taper on the polypropylene sections, and the dielectric constant and length of the quarter-wave matching sections. Some preliminary measurements were made with just polypropylene sections to determine if the taper angle was critical. The result was that the taper appeared to be quite un-critical, so a simple 30 degree taper was used for most of the remaining measurements.

The best results obtained by optimizing the length and dielectric constant (in discrete steps, since only a limited number of materials were available for fabrication) we obtained a flange to flange transmission loss of -3 dB. This is about half of the flange to flange loss measured using

the values that were used in the original measurement of the 94 GHz directional coupler modulator and the bow-tie Mach-Zehnder modulator demonstrated under the previous contract.

4.4 MODEL TEST RANGE

The back-to-back arrangement described above is satisfactory for optimizing the efficiency of the waveguide to lithium niobate slab guide, but it tell us nothing about the efficiency of coupling from the slab guide to the antennas in the modulator. For this reason we undertook to make a model test range that would include all the elements, but at a frequency of 10 GHz rather than mm-waves, so that the parts would be big enough to fabricate easily.

The test range is shown schematically in Fig. 4.1. A 24" by 54" aluminum sheet is used as the support for Emerson and Cummins Stycast® artificial dielectric material that simulates the lithium niobate modulator substrate and input slab waveguide. The tapered polystyrene slab waveguide is fed by a machined horn coupled to a standard WR-90 waveguide. A precision coax fitting is positioned under the "substrate" section just at the surface to connect to an antenna on the substrate surface. The coax fitting is mounted in a removable section of the plate so that it may be easily interchanged, for example, to change from one antenna to several antennas, for example.

With this test range, we should be able to measure the overall efficiency of coupling from the source waveguide to the center of the antenna. Unfortunately, the contract ended before any significant measurements could be made. We hope to be able to use this range in the future to examine antenna alternatives, such as the V antennas described in the next section.

4.5 R-F COUPLING REFERENCES

4.1 E.A.J. Marcatili, "Dielectric Rectangular Waveguide and Directional Coupler for Integrated Optics", Bell System Technical Journal, vol. 48, pp. 2071-2102, September 1969

4.2 T. Moreno, *Microwave Transmission Design Data*, Artech House, Inc., 1989, pp. 51-53

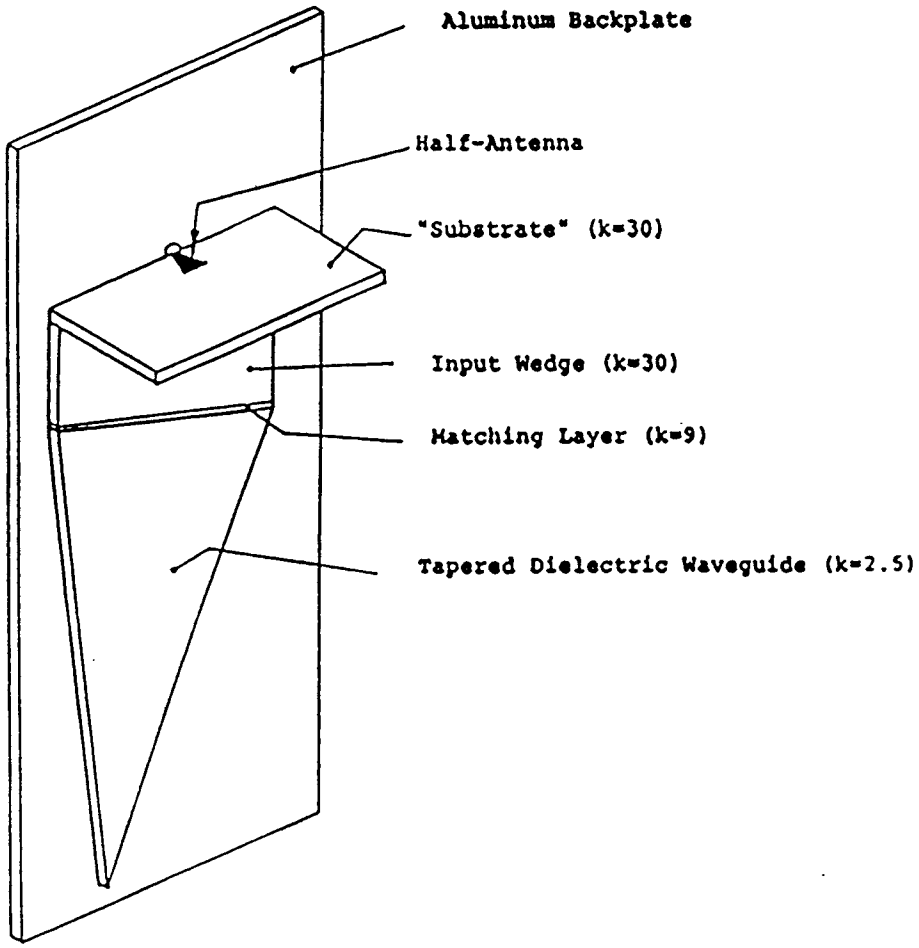

Fig. 4.1 10 GHz Scale Antenna Test Range

5.0 V ANTENNAS FOR ANTENNA-COUPLED MODULATORS

In past demonstrations, resonant dipoles and broadband bow-tie antennas were used as the basic elements for our antenna-coupled modulators. During the present program, we also looked at the possibility of using antennas with gain to improve the performance of the modulators by improving the coupling of the illuminating field to the antennas. Our attention was focused on the "V" antenna, since this seemed like the simplest antenna to understand. Unfortunately, no previous theoretical (or experimental) treatments of V antennas on a dielectric interface seem to exist. Thus, we sought to understand such antenna from first principles. The material below is a brief summery of our conclusions, with Appendix A taken intact from F. T. Sheehy's Ph. D. dissertation [Ref. 5.1] providing the theoretical reasoning and examples of radiation patterns.

5.1 ANTENNAS ON A DIELECTRIC HALF-SPACE

Since the electrodes of the antenna-coupled modulator are on the surface of the $LiNbO_3$ electro-optic material, the antennas will be on the interface between a high dielectric constant region and air. The behavior of the antenna is changed fundamentally by the presence of a dielectric interface like this. The simplest way to look at this effect is to assume that the $LiNbO_3$ is infinitely thick and examine the behavior of antennas on a dielectric half-space. A number of papers have been written on various aspects of this [Refs. 5.2 - 5.7] for simple dipoles. Based on the physical insight derived from these references, we can estimate the radiation patterns of V antennas on a dielectric interface.

An antenna on a dielectric half-space must have a radiation null in the direction of the interface, because no TEM wave can propagate along the dielectric interface. The phase velocities are different in the two media on either side of the interface, and thus the phase fronts cannot match at the boundary. The other striking feature of such an antenna is that most of its power goes into the dielectric rather than into the air. Rutledge et al. [Ref. 5.7] have given an

explanation of this by considering the antenna as a receiving antenna. The antenna is at the interface between a low-impedance medium (the dielectric) and a high-impedance medium (air). Any power incident on the interface from the air-side will be reflected from a low-impedance medium. When this happens, the electric field-strength is small at the interface and the antenna response is small. When the power is incident from the dielectric side it is reflected from a high-impedance medium, so the electric field-strength is high at the interface and the antenna response is large.

Examples of the antenna patterns of interfacial dipoles are illustrated in Figs. 5.1 and 5.2. The equations from which these patterns are derived are given in Appendix A. Figure 5.1 shows the H-plane pattern of a dipole on a half-space of dielectric constant $\varepsilon = 4$. (The antenna is normal to the plane of the diagram.). Note that there is very little coupling to the air-side of the interface. Almost all of the power is radiated into the dielectric.

A notable feature of the antenna pattern is the cusp in the pattern on the dielectric side. This cusp occurs at the critical angle, i.e., at about 30° in this case. Figure 5.2 is again a H-plane pattern of a dipole, but this time on a high-dielectric material, $\varepsilon = 36$. This time there is virtually no coupling at all to the air-side of the interface. The cusp occurs at 9.6° now. If the length of the antenna is increased, and it is bent to form a V-antenna, quite different antenna patterns are possible.

5.2 THE V ANTENNA ON A DIELECTRIC HALF-SPACE

Figure 5.3 shows the H-plane pattern of a V-antenna on a dielectric half-space of $\varepsilon = 28$. Again, the equations for this pattern are given in Appendix A. In this case the length of each arm of the V is increased to one wavelength from end-to-end at the interface, where the effective relative permittivity for propagation along a wire antenna or a transmission line is taken as the mean of the permittivities of the two media: $\varepsilon_{EFF} = (28 + 1)/2 = 14.5$ and the effective refractive index is thus $(14.5)^{1/2} = 3.8$. The V angle is 100°. This figure is taken from

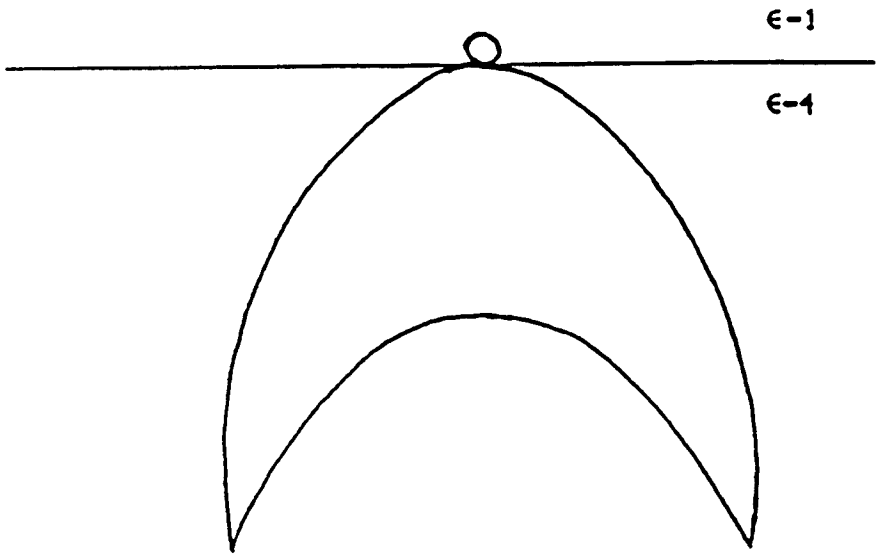

Fig. 5.1 H-plane pattern of a straight dipole on a dielectric half-space with $\varepsilon = 4$.

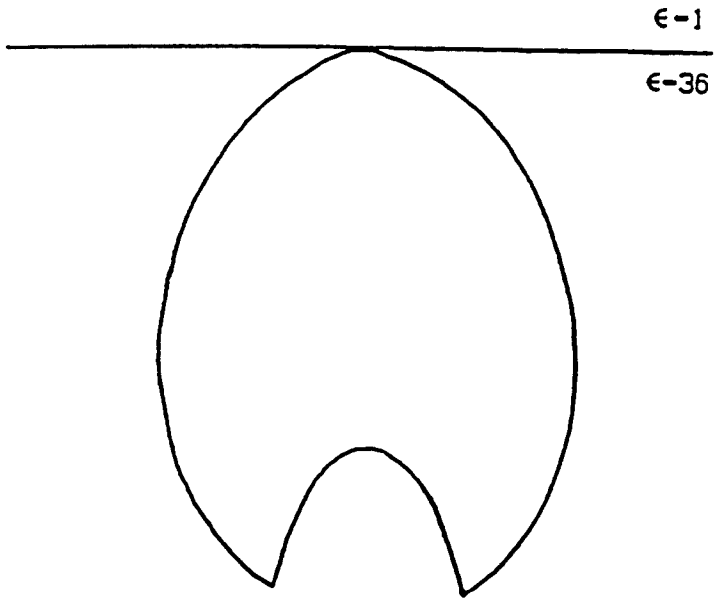

Fig. 5.2 H-plane pattern of a straight dipole on a dielectric half-space with $\varepsilon = 36$.

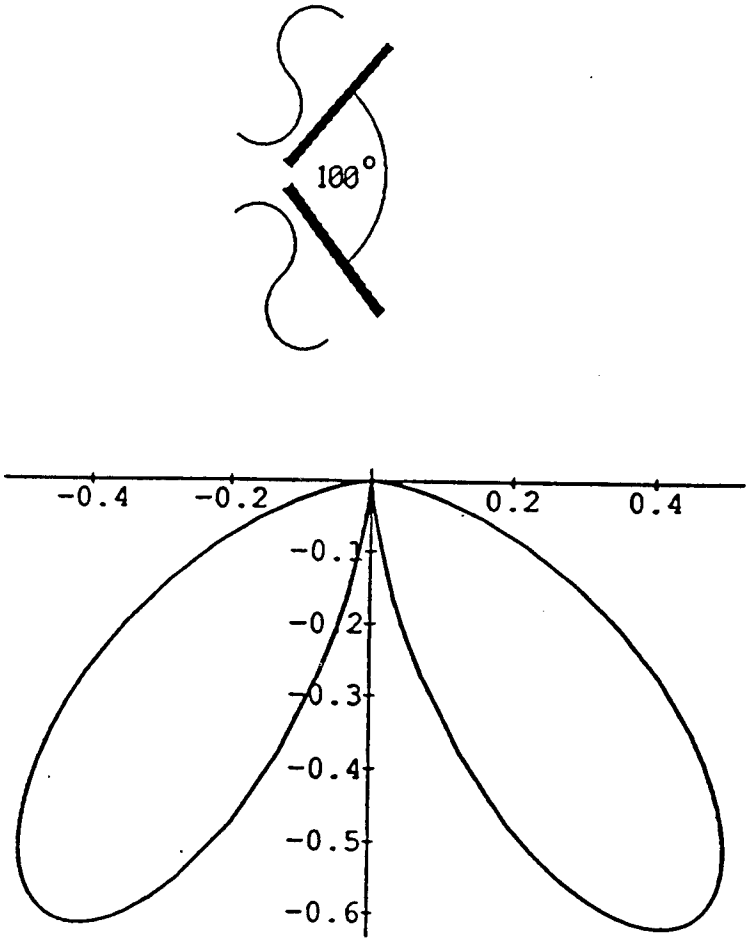

Fig. 5.3 Antenna pattern of a V antenna on the surface of a dielectric with $\varepsilon = 28$. Each arm of the V is one surface-wavelength long. The V angle is 100°. The pattern shown is in the dielectric, in the plane which bisects the V angle.

Appendix A, which gives the equations for radiation patterns for wire antennas on dielectric half-spaces. As we have noted before, the fact that the antenna couples more efficiently into the dielectric than into the air is a fortuitous one, since the modulating signal must be incident on the antenna array from inside the dielectric in order to achieve the necessary phase-velocity-match condition. This fits in nicely with the antenna's preference for radiation coming from inside the dielectric.

While the gain of this antenna over a dipole was not calculated explicitly, it is clear from the pattern that it would give a significantly improved performance over a simple dipole. It is an excellent candidate for future use in antenna-coupled modulators, and we intend to try it. We did not try to build modulators using V antennas under this contract, however, because an even more intriguing possibility arose during the study of this antenna, and that candidate, the "slot-V" antenna was pursued instead. It is described in the next section.

We should make a final note on the V antenna. If the V elements are made of thin conductors, then the antenna will be resonant and bi-directional. (The bi-directionality is clearly shown in the pattern of Fig. 5.3.) Making the conductors "fatter" will increase the bandwidth, as in ordinary dipoles. And just as in ordinary dipoles, the V can be broad-banded by using fan-shaped conductors as in the "bow-tie" antenna already demonstrated. For that antenna, the V becomes more unidirectional in the direction of the enclosed angle, since the traveling waves on the elements are not reflected from the open-circuited far ends of the elements. This would be the preferred embodiment of the V antenna, even though no exact analysis exists for it.

5.3 V-ANTENNA REFERENCES

5.1 M. Kominami, D.M. Pozar, and D.H. Schaubert, "Dipole and Slot Elements and Arrays on Semi-Infinite Substrates," IEEE Trans. Ant. & Prop., vol. AP33, No. 6, pp. 60O-607, June 1985.

5.2 N. Engheta and C.H. Papas, "Radiation Patterns of Interfacial Dipole Antennas," Radio Science, vol. 17, pp. 1557-1566, November-December 1982.

5.3 G.S. Smith, "Directive Properties of Antennas for Transmission into a Material Half-Space," IEEE Trans. Ant. & Prop., vol. AP-32, No. 3, pp. 232-246, March 1984.

5.4 R.C. Compton, R.C. McPhedran, Z. Popovic, G.M. Rebeiz, P.P. Tong, and D.B. Rutledge, "Bow-Tie Antennas on a Dielectric Half-Space: Theory and Experiment," IEEE J. Ant. & Prop., vol. 35, No.6, pp. 622- 631, June 1987.

5.5 D.B. Rutledge, D.P. Neikirk, and D.P. Kasilingam, "Integrated-Circuit Antennas," Chapter 1 in *Infrared and Millimeter Waves, Vol. 10,* Academic Press, 1983.

6.0 THE SLOT-V ANTENNA-COUPLED MODULATOR

In this section we present a new antenna-coupled modulator configuration, conceived by F. T. Sheehy before the present program began. The idea seemed sufficiently novel to file for a patent, and one has now issued [Ref. 6.1]. The modulator is novel in that the $LiNbO_3$ modulator substrate is, itself, used as a dielectric slab wave to guide the input signal to the antenna array, rather than using a separate slab waveguide normal to the modulator chip to couple the signal in. What required for this configuration is an antenna that has the maximum of its radiation pattern directed along the interface, rather than directed down into the substrate, like the dipoles and V antennas described in Section 5. Such an antenna is the "Slot-V" described below.

6.1 THE SLOT-V ANTENNA

In the course of analyzing ordinary V antennas on a dielectric interface, we became interested in the *complement* of the V antenna, the "Slot-V," in which the V elements are replaced by slots in a conducting plane covering the entire dielectric interface. This antenna is shown schematically in Fig. 6.1, where it is compared with an ordinary V antenna with tapered elements. For the slot-V antenna, the entire substrate (dielectric - air interface) is covered with a conducting surface. The V elements are then apertures in that conduction surface. The reason this antenna can have its maximum radiation *along* the dielectric interface is due to the conducting surface, which "shields" the two sides of the interface from each other. Thus the restriction that a null in the radiation pattern must in the direction of the interface because the phase fronts will not "match" across this boundary is removed, since the conductor isolates waves on the two sides of the boundary from each other. Thus the slot-V seems like the ideal antenna to couple to waves propagating in the modulator substrate used as a slab waveguide.

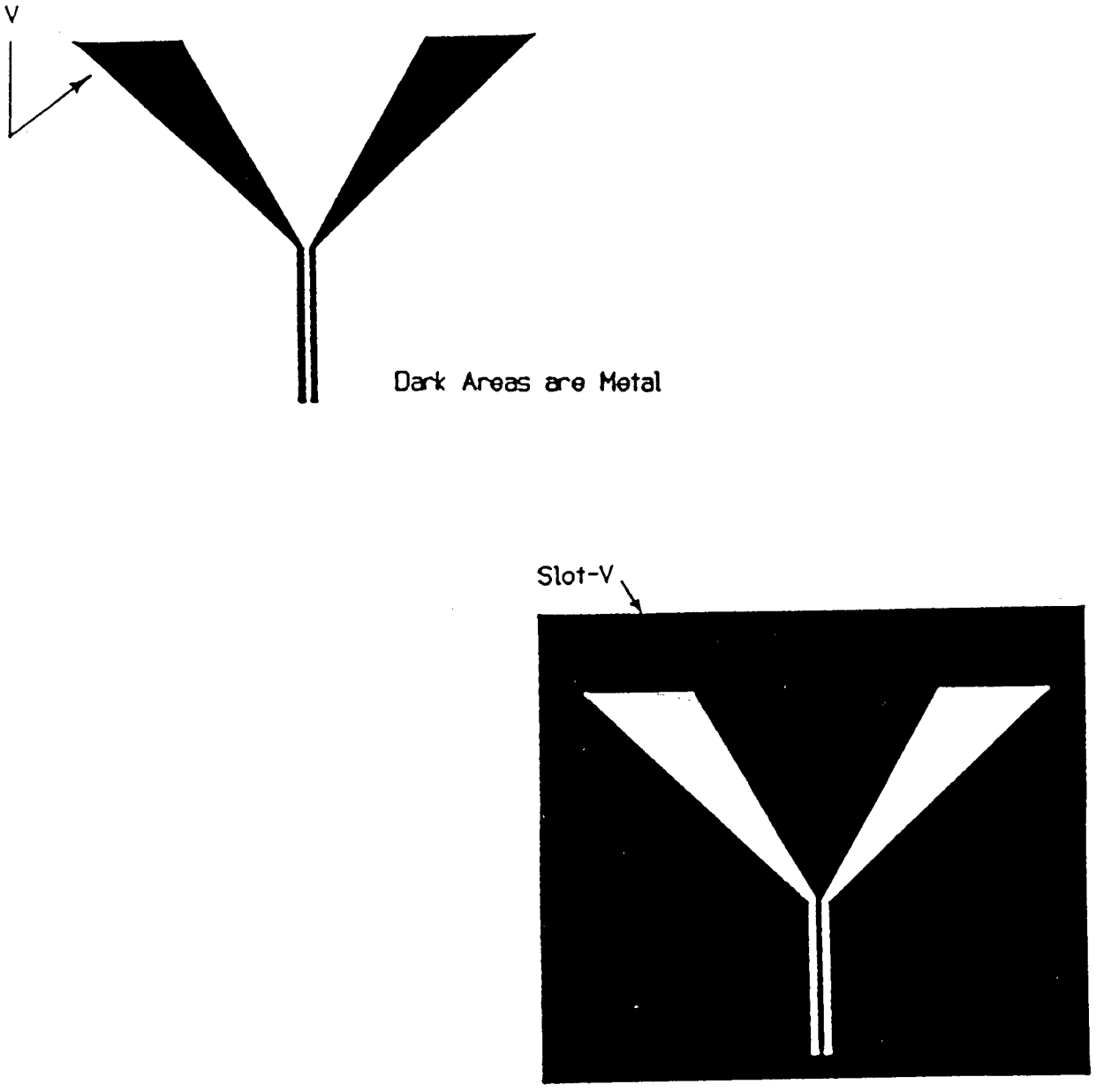

Fig. 6.1 A V antenna and its complement, the Slot-V antenna. Note that the V antenna is fed with a two-conductor line, while the Slot-V antenna is fed by a co-planar "coaxial" line.

Radiation pattern measurements and other features of the slot-V antenna have been measured recently by A. Moussessian in another research group at Caltech, and reported at a recent meeting [Ref. 6.2].

Note that the slot-V antenna can be fed from planar "coax", as shown in Fig.6.1. This makes an ideal fit to the two optical waveguides of the Mach-Zehnder modulator, provided the waveguide separation can be made equal to spacing of the two gaps of the planar coax. That separation, along with the width of the center conductor, determines the characteristic impedance of the coax, which should ideally be matched to the drive point impedance of the antenna. These design considerations are described below.

Of course, now some other means must be used to obtain the proper antenna-to-antenna phase delay to provide the phase velocity matching. The answer to this was found by again tilting the illumination with respect to the optical waveguide, but this time *in the plane* of the modulator chip. The resulting geometry is described below.

6.2 THE SLOT-V MODULATOR CONFIGURATION

Successive antenna-couple segments must be driven in the proper phase to match the phase velocity of the optical waveguide. The solution to this is to rotate the V antennas with respect to the transmission line segments, as shown in Fig. 6.2, using a "bend" in the transmission line to connect the straight section aligned with the optical waveguides to the antenna. Now the antenna array can be angled with respect to the optical waveguide as shown in Fig. 6.3 (a top view of the $LiNbO_3$ modulator chip) and illuminated by a wave incident on the edge of the chip. The proper angle is the same as before (using the correct value for the permittivity of $LiNbO_3$ of 28 or 41, depending on the crystal orientation).

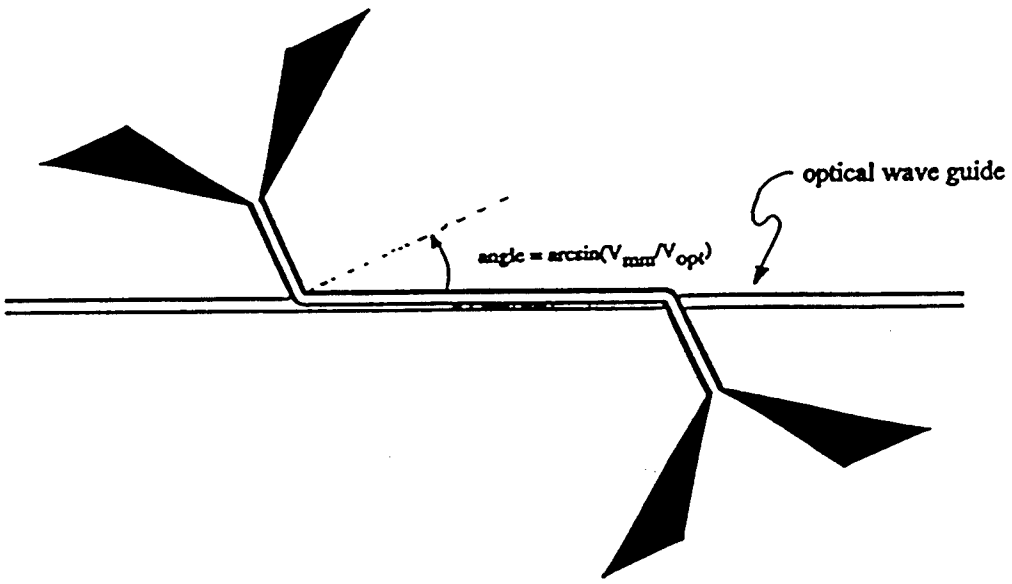

Fig. 6.2 Slot-V antenna coupled to a transmission line segment. A transmission line bend is used to allow the antenna to "look" in a direction different than the straight section of the transmission line, and a second slot-V antenna is used as a radiative matched termination.

In Fig. 6.3 the underlying modulator is assumed to be a Mach-Zehnder amplitude modulator. Such a modulator requires provision for d-c bias. In our previous experimental work with Mach-Zehnder modulators we applied d-c bias to the antenna/modulator segments themselves. Here, we use an alternative method, where the d-c bias is achieved using separate electrodes reserved for the purpose. This removes the need to provide for d-c bias to each antenna/electrode segment.

Note that the configuration of Figs. 6.2 and 6.3 provides the solution to a difficulty encountered in our previous structures, that of terminating the transmission line segments in their characteristic impedance to avoid resonant behavior. Since we can "point" the slot-V antennas in any direction, we simply terminate the transmission line segments in a second slot-V antenna and "point" it towards a dummy load at the opposite edge of the modulator chip. Thus the transmission line segments behave as a true traveling wave modulator instead of exhibiting a standing wave caused by the previous "open circuit" condition at the far end of the line.

In our previous experimental modulators the modulating signal was radiated onto the antenna array through the substrate. This required a signal feed structure in a plane normal to the modulator substrate. In the structure shown in Fig. 6.3, however, the modulating signal propagates in the substrate as a guided wave. This requires a feed structure in the same plane as the modulator substrate. From a practical point of view, this should result in an overall structure that is rugged and more convenient to build. The modulator substrate will be metal-covered (except for the antenna and transmission line slots), so the dielectric waveguide formed by the substrate will now have one metal boundary, making it a dielectric slab *image* guide, rather than a symmetric dielectric slab guide. The transition to ordinary waveguide must also have this image symmetry, and that is easily satisfied by a "half waveguide" driving a "half horn transition" , as shown in Fig. 6.4. The metallic image plane can thus serve as the mechanical support for both the modulator and feed system. The $LiNbO_3$ modulator substrate can be bonded to the backplane by the "flip-chip" technique used in semiconductor devices.

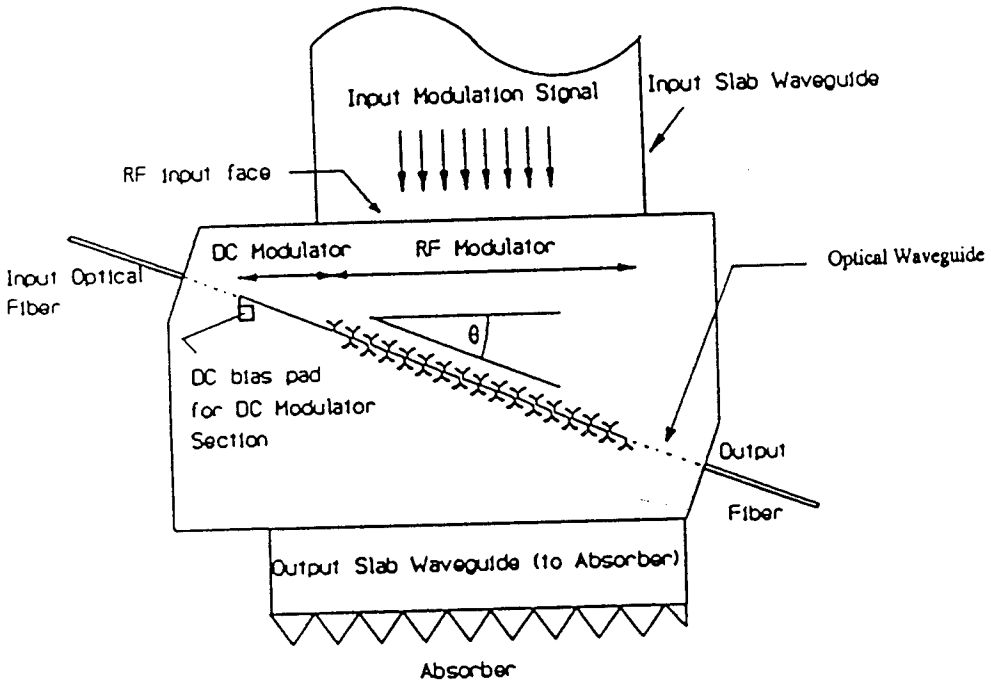

Fig. 6.3 Top view of the modulator chip, showing the array of antenna/transmission line segments of Fig. 6.2 illuminated from the top edge of the chip, with the optical waveguides aligned along the direction of the MZ optical waveguides.

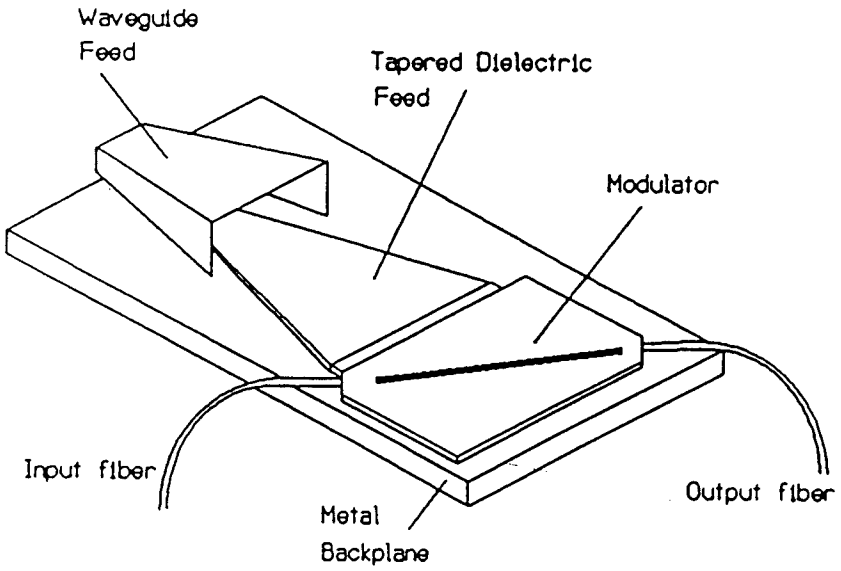

Fig. 6.4 Mechanical structure of the Slot-V modulator, showing the underlying metal backplane support, with the $LiNbO_3$ modulator with the metal covered interface "flip-chip" bonded to it. Small cavities in the backplane keep it from shorting out the slot antennas and the transmission lines.

6.3 SLOT-V MODULATOR DESIGN

When Sheehy graduated in June 1993, the slot-V modulator existed on paper only, in his patent application [Ref. 6.1] and in his Ph. D. dissertation [Ref. 6.3]. Subsequently, Lee J. Burrows, a new graduate student with the group, took up the task of designing and demonstrating this modulator. The first task was the determination of the proper slot-V antenna and transmission line segment dimensions. The slot-V dimensions were scaled from work by Moussessian. The transmission line dimensions were determined to match the antenna impedance predicted by Moussessian [Ref. 6.2] for the slot-V, using the techniques described by Gupta [Ref. 6.4]/

The resulting electrode mask (LJB-el-1) is shown in Figs 6.5. We decided to make modulators at 100 GHz, 94 GHz and 20 GHz, primarily because we have signal sources in these three bands. The 20 GHz modulator can be considered as a "large scale model" that might be useful in optimizing the feed structure with less precise mechanical tolerances. A waveguide mask (LJB-wg-1) was also designed with simple Mach-Zehnder modulators aligned to each modulator. The waveguide dimensions were chosen for operation at 1.3 microns wavelength using the titanium in-diffusion process. The masks were fabricated at Align-Rite, and sent to Hughes Research Laboratories for fabrication. Unfortunately, the present contract expired before the modulator substrates were received back from HRL.

6.4 PRESENT STATUS OF THE SLOT-V MODULATOR

Work on the slot-V antenna coupled modulator has continued, albeit at a much slower pace, since the end the contract. A first sample of the modulator substrate was completed at HRL, and diced into individual modulators, with the ends finished to an acceptable degree by using a precise dicing saw at HRL. Some work on optimizing the tapered dielectric image line feed system was undertaken at 20 GHz, so that a proper backplane could be designed. This work is continuing.

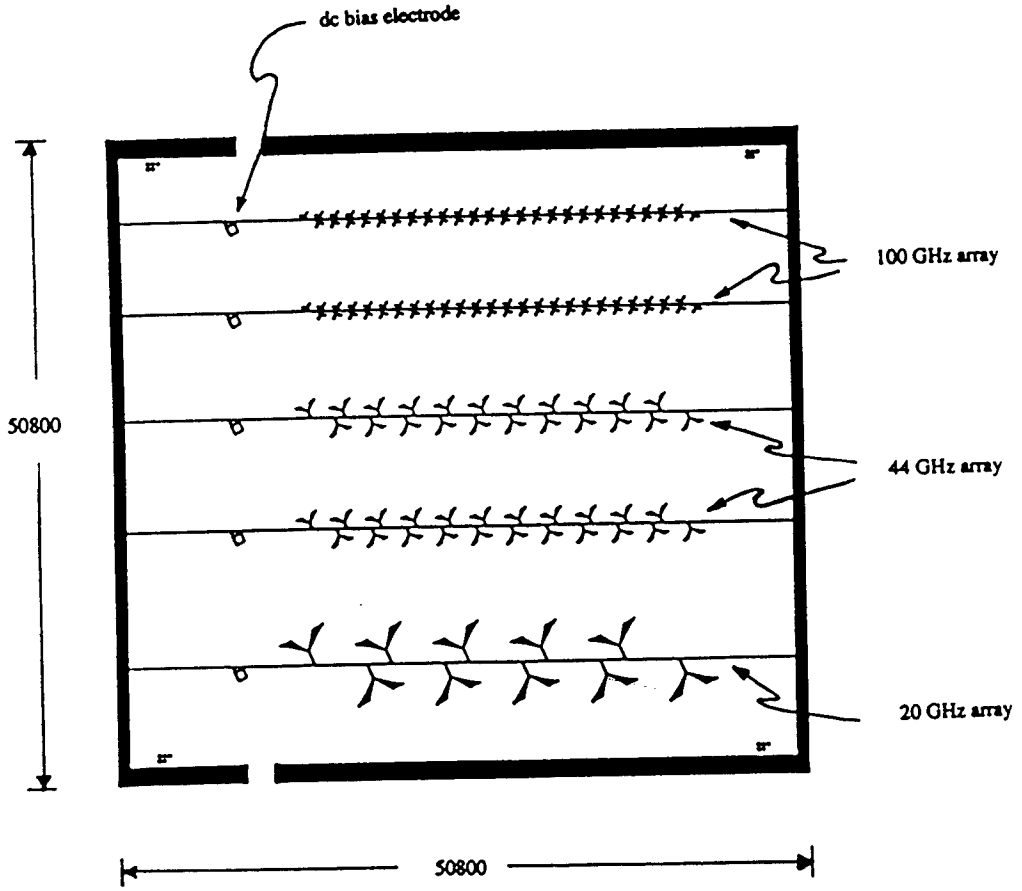

Fig. 6.5 View of the Mach-Zehnder modulator mask. Note the d-c bias electrodes at the beginning of each antenna array. The $LiNbO_3$ substrate produced from this mask is subsequently cut to create a separate modulator from each array.

6.5 SLOT-V ANTENNA REFERENCES

6.1 F. T. Sheehy, U. S. Patent No. 5,309,531, issued May 3, 1994, assigned to the California Institute of Technology.

6.2 A. Moussessian and D. B. Rutledge, "A Millimeter-Wave Slot - V Antenna," Proc. IEEE AP-S International Symposium, Chicago Illinois, 18 - 25 July 1992.

6.3 F. T. Sheehy, "Antenna-Coupled mm-Wave Electro-Optic Modulators and Linearized Electro-Optic Modulators," Ph. D. dissertation, California Institute of Technology, June 1993.

6.4 K. C. Gupta, Ramesh Garg, and I. J. Bahl, *Microstrip Lines and Slotlines,* Artech House, 1979, pp. 257-265

7.0 WAVEGUIDE FABRICATION

During this program, we looked at the feasibility of fabricating our own optical waveguides in lithium niobate, rather than continuing to depend on the generosity of the Hughes Research Laboratories to fabricate them for us. However, we wished to do more than simply duplicate the facilities available at Hughes. Since HRL used exclusively the titanium in-diffusion waveguide fabrication method, we decided to investigate an alternative fabrication procedure, that of proton exchange. This method is used in commercial practice by Uniphase Telecommunications Products, a division of Uniphase, Inc. (UTP, formerly known as United Technologies Photonics), who holds the major patents on it. This method can be implemented with much lower temperature diffusion furnaces, so it was much less expensive for us to acquire the necessary capability. We also hoped to compare the relative merits of the two methods, keeping the other factors in the modulators the same.

Coincidentally, Professor Axel Scherer joined the Caltech faculty early in the present program. Professor Scherer is an expert in semiconductor micro-device fabrication, and has all the photolithographic facilities that we would also need in fabrication of not only the waveguides, but the entire modulator at Caltech. He has been very generous with his time and facilities in this program, and that has provided an additional incentive to undertake this task.

An extensive literature search was undertaken to find out what was already known about proton exchange waveguide formation. This proved very interesting and helpful, both for what was in the literature and also for what was claimed, but not fully explained by those most successful in making proton-exchange waveguides. Thus, our interest became a quest for those "trade secrets" as well as knowledge of the basic physics of the process.

We summarize our views on proton exchange waveguides below. But first we review briefly the other techniques for waveguide formation in lithium niobate as background.

7.1 EARLY $LiNbO_3$ WAVEGUIDE TECHNIQUES

7.1.1 FORMED BY OUT-DIFFUSION OF Li_2O

Waveguides were first fabricated in lithium niobate through out-diffusion of lithium oxide (Li_2O) by Kaminow *et al.* [Ref. 7.[1]] This was accomplished by annealing the lithium niobate at 900 °C to 1100 °C in a vacuum or oxidizing ambient gas for several hours. Lithium niobate is able to crystallize in a non-stoichiometric form, $(Li_2O)_x(Nb_2O_5)_{1-x}$, hence allowing the lithium to readily diffuse out of the crystal. The ordinary index of refraction, n_o, is not affected by this process, while the extraordinary index of refraction, n_e, increases linearly as the fraction x in the crystal decreases with diffusion. These out- diffused waveguides supported only TE modes because only the extraordinary refractive index was altered by this process.

7.1.2 FORMED BY ION IMPLANTATION

Optical waveguides may also be produced in lithium niobate with the addition of impurities by ion implantation. This is executed by bombarding the substrate with high energy (i.e. 7 keV to 2 MeV) ions such as Ar, H, He, N, Ne, O, or Ti. These ions pervade the surface of the substrate and loose energy through nuclear collisions and electronic excitation. The result is a surface layer that is slightly damaged, separated from the bulk substrate by an amorphous region with a lower index of refraction than that of the substrate. The benefits of waveguides made by this procedure are: large index of refraction changes, adequately large electro-optic coefficients, and reliable waveguide reproducibility.

The amorphous section is typically formed 2 to 4 microns below the surface and is a few microns thick. The amount of index change depends on nuclear collisions, but as an example, the maximum refractive index changes in a y-cut sample are $\Delta n_e = -0.105$ and $\Delta n_o = -0.165$. The temporal stability of these changes depend on the kind of ion implanted and the

temperature at which the process takes place [Ref. 7.[2]]. After the implantation, samples are usually annealed at temperatures near 200 °C. This is a necessary step to remove radiation damage from the optical guiding layer, and after annealing, optical losses have been reported to be as low as 0.2 dB/cm [Ref. 7.[3]].

Several drawbacks have yet to be overcome with this method of waveguide fabrication. Some of these are: (1) As the ion dose increases, the electro-optic effect of the guiding region decreases, (2) The lithium niobate outside the implantation area is also degraded, and (3) Perhaps worst of all, stress and defects are induced into the crystal due to the implantation process. And, of course, ion implantation is not an inexpensive process, and is not preferred for mass production.

7.1.3 FORMED BY METAL ATOM IN-DIFFUSION

The in-diffusion of metals alters the refractive index of lithium niobate, with different metals producing differing signs and magnitudes of the resulting change. Usually, a thin film of the diffusing metal is laid down above the desired waveguide region by sputtering or evaporation. The sample is then heated to between 800 °C and 1100 °C in reactive or inert atmospheres. Diffusion rates of the different metals are dependent on the orientation of the diffusion direction, so that the optimum heating times and temperatures vary with the metal used and the axial cut of the lithium niobate. Divalent metals, such as Ni, Zn, and Mg, substitute for lithium atoms. Typically this causes a *reduction* in the *extraordinary* index of refraction. Mg also causes a *decrease* in the *ordinary* index of refraction, while Ni and Zn cause an *increase*. Trivalent and tetravalent metals, such as Fe, Cr, and Ti, substitute for niobium in the crystal lattice, resulting in an *increase* in both the *extraordinary and the ordinary* indices. By far, the most useful metal atom in-diffusion has been titanium, and its properties are described in the next section.

7.2 WAVEGUIDES FORMED BY TITANIUM IN-DIFFUSED

Titanium in-diffused waveguides were first fabricated in 1974 by R. Schmidt *et. al.* [Ref. 7.[4]]. This process is currently widely used to form low-loss slab and strip waveguides, and particularly, it is used at HRL and in all our modulators at Caltech to date. These waveguides have good optical confinement because of the comparatively large increases in both the ordinary and extraordinary refractive indices ($\Delta n_e < 0.04$ and $\Delta n_o < 0.02$). Accordingly, titanium in-diffused optical waveguides will support both TE and TM modes. Titanium in-diffusion has been studied extensively, yet the correspondence between fabrication procedure and waveguide characteristics is not completely understood. One particularly troublesome unresolved problem with this type of waveguide is a small, long term instability of the optical characteristics. There is also some continuing argument over the relative size of the photorefractive effect ("optical damage") suffered in Ti waveguides in lithium niobate relative to proton exchange guides in lithium niobate or Ti waveguides in lithium tantalate. Different laboratories seem to obtain different, conflicting results.

Titanium in-diffused waveguides, although extensively used, are not trivial to fabricate because of the high processing temperature and its possible side affects on the bulk lithium niobate. One widely seen problem is the out-diffusion of Li_2O. As mentioned above, out-diffusion of Li_2O causes a change in index of refraction, which manifests itself as an overall surface guiding region which can act on the optical TE mode. When this Li_2O out-diffused layer overlaps the Ti in-diffusion waveguide, single-mode propagation is prevented. One method of countering the Li_2O out-diffusion is by performing the titanium in-diffusion in an Li_2O-rich atmosphere. Another method is to maintain a water vapor rich atmosphere (gaseous O_2 flowing through pure H_2O held at 80° to 90° C) during in-diffusion, which inhibits the formation of and decomposes the $LiNb_3O_8$ phase.

7.3 PROTON EXCHANGE WAVEGUIDES

Proton exchange in lithium niobate is an attractive method of fabricating low-loss optical waveguides. It was first demonstrated by Jackel *et. al.* in 1982 [Refs. 7.[5], 7.[6]], and essentially is the conversion of $LiNbO_3$ to $Li_{1-x}H_xNbO_3$ by in-diffusing hydrogen atoms. Submerging the lithium niobate crystal into a proton source, such as an acid (e.g., benzoic or citric), a hydrate melt or even water, at moderate temperatures (less than 200 °C) causes proton exchange to occur, and it occurs quite rapidly. Proton exchange induces non-isotropic refractive index changes, with typically large values of $\Delta n_e = 0.12$ and $\Delta n_o = -0.04$ (at λ=0.63nm). The fact that the change in the ordinary index is negative means that light polarized along the ordinary direction is not guided. Therefore, only light polarized along the c-axis of the crystal will propagate, meaning only TM modes for z-cut $LiNbO_3$, and only TE modes for x-cut $LiNbO_3$. The proton exchange waveguides typically exhibit relatively high optical losses, on the order of 3 dB/cm to 6 dB/cm.

Unfortunately, the exchange process also leads to a degradation of the electro-optic effect of the crystal (bulk $LiNbO_3$ $r_{33}=30*10^{-12}$ m/V, after exchange, $r_{33}=3*10^{-12}$ m/V) and temporal optical instabilities.

Fortunately, annealing the waveguides after they have been formed improves these undesired effects. Post processing annealing results in the recovery of the electro-optic coefficient, lower propagation losses (on the order of 0.15 dB/cm [Ref. 7.[7]]), and temporal stability. Why annealing does this is explained below.

7.3.1 REFRACTIVE INDEX CHANGE WITH PROTON EXCHANGE

When protons replace lithium in the crystal, a modification of the index of refraction occurs, but the overall change results from a variety of contributing factors. Since a proton, H^+, is smaller than a lithium ion, Li^+, replacement likely causes a tensile stress at the surface of the

crystal. However, the magnitude of this stress is small because H^+ is only *slightly* smaller than Li^+. The resulting small surface stress will contribute to a small, *negative* Δn_o. The difference in polarizability of the exchanging ions also affects the refractive index. Since the polarizability of Li^+ is small and that of H^+ is identically zero, this will also cause a slight *negative change in* Δn_o and leave Δn_e *unaltered.* A change in the molar density and volume caused by the ionic replacement is also expected, since H^+ is smaller than Li^+. This change will cause a small *increase in the extraordinary refractive index.* However, the major contributor to the *large extraordinary refractive index increase* likely comes from a change in crystal polarization caused by differential site preference of the exchanging ions in the lattice, as suggested by C. E. Rice [Ref. 7.[8]]. Rice proposes that the exchanged H^+ ions reside in the oxide planes, while the Li^+ ions had been located in the lattice octahedral sites. Replacement of Li^+ by H^+ then results in the displacement of positive charge along the c_h axis, moving it from one triangular face of the octahedral site into the opposite face. This charge movement may increase the polarizability of the oxygen more distant from the proton, while decreasing the polarizability of the closer oxygen. Rice believes that this explains the increase in n_e, along the c_h axis, and the decrease in n_o, perpendicular to c_h. Experimental results of Rice and Jackel [Ref. 7.[9]] support this theory. They report lattice parameter measurements indicating that the change in c_h is very small, while the change in a_h is large. Minakata *et. al.* [Ref. 7.[10]] have reported on proton exchange melts with $0 < x < 2.5$, that there is a high amount of strain $\Delta c_h/c_h$ and negligible strain $\Delta a_h/a_h$, which also points to the change in c_h affecting Δn_e.

7.3.2 PHASE STRUCTURE OF LITHIUM NIOBATE

At temperatures between 0 °C and approximately 200 °C, lithium niobate exists in a single crystalline phase which exhibits low optical loss and an excellent electro-optic coefficient. When a small number of protons are exchanged for the lithium atoms, the material remains a single-phase structure (designated α in the literature) for proton replacement up to the fraction $x = 0.12$. For higher fractions, $0.12 < x < 0.55$, an additional phase, β, can coexist, and is undesirable in three ways: the proton mobility in β-phase lithium niobate is higher (which we

hypothesize can result in bias drift in an electro-optic device), the optical losses are higher (the optical wave experiences refraction and scattering at the α/β phase boundaries), and the electro-optic coefficient is thought to be smaller (on theoretical grounds... no experimental measurements are known). For still higher fractions, $x>0.55$, several other phases, β', β'', β''', γ..., can also coexist, all with largely undetermined (but likely undesirable) electro-optic properties. At $x = 1$, $HNbO_3$, the crystal structure is cubic, and the material exhibits no electro-optic effect.

In the standard proton exchange fabrication process, the fraction x is typically greater than 0.5 at the end of the acid immersion step. It is not practical to make it smaller, since the proton exchange takes place so rapidly. An alternate procedure using a mixture of benzoic acid and lithium benzoate has been shown to slow down and control the exchange, but is not used commercially because of the diffusion then takes a prohibitively long time. The undesired high concentration of protons following the simple exchange, which results in a mixture of α and β phases, is then reduced to the desired value of x, to realize the pure α structure, by annealing for some time at a temperature *higher* than the diffusion temperature (typically 300 °C to 400 °C for hours). The trick in this process is to end up with the *proper value of x*, which also determines the refractive difference, Δn, between the waveguide and the surrounding material, and the desired size of the waveguide, all in the pure α crystal structure. If any of the β phase regions remain within the optical guiding region, they will likely become a serious source of instability in the refractive index and the electro-optic coefficient and result in a drift in the optical phase shift through the guide. The transition $\alpha \longleftrightarrow \beta$ is a *second-order* phase transition and thus requires no input of energy to occur: Simply having $x > 0.12$ is sufficient to cause the phases to interchange in time at room temperature. Temperature changes and applied fields will hasten such transitions.

7.4 PROTON EXCHANGE WAVEGUIDE EXPERIMENTS

We began our work on proton exchange waveguides approximately one year into the present contract. Even before we surveyed the literature fully, we began a small project to fabricate proton exchange waveguides to test the feasibility of doing the processing at Caltech. The initial test samples of proton exchange were done with straight waveguides of 4, 5, and 6 micron widths on scrap pieces of lithium niobate. We used the benzoic acid processing described by Clark, et al.[Ref. 7.[1]1]. The end faces of these pieces were polished at Hughes Research Labs and measured at Caltech and HRL They exhibited transmission characteristics roughly equivalent to titanium in-diffused waveguides. These nascent results encouraged us to continue our experiments. We decided to compare different proton exchange processes and eventually look into the annealing procedure also. Our initial experiments also made clear the need for a furnace with accurate electronic control of temperature ramp-up and ramp-down. Subsequently, we purchased such a furnace with Caltech funds.

Before proceeding with further experiments, we reviewed over 50 articles and noted the various recipes for the fabrication of proton exchange waveguides. We also developed some definite ideas about the annealing process and how it works, as described above. We were particularly interested in specific disadvantages associated with ordinary proton exchange guides (i.e. large propagation losses, temporal refractive index instabilities, and the decrease of the electro-optic effect) that are apparently reduced by annealing.

We began the second round of our experimental work by designing a new waveguide mask (LJB-wg-2) consisting of many straight waveguides of varying width. The mask was received too late in the program to carry out the actual proton exchange experiments, however.

7.5 STATUS OF PROTON EXCHANGE STUDIES

After the program end date, we received the straight waveguide mask and used it to make a lithium niobate substrate with a protective metal coating needed as a proton exchange mask. This substrate has been diced into many separate sections of straight waveguide. We are currently subjecting these sections to various schedules of time and temperature of proton exchange and will then add a series of annealing schedules before measuring their optical transmission.

Also following the end of the present program, we considered a number of material techniques to try to distinguish α and β phases and their properties. We believe that transmission electron microscopy may be able to make this distinction. Accordingly, Lee Burrows has undertaken the task of learning sample preparation and use of the transmission electron microscope in Prof. Axel Scherer's lab. We also have made some preliminary Kikuchi pattern measurements of samples than may allow us to distinguish different amounts of proton exchange in lithium niobate samples. The results to date are encouraging, but much more needs to done. Again, these measurements are being made in Prof. Scherer's lab by Lee Burrows.

7.6 WAVEGUIDE FABRICATION REFERENCES

7.1 Kaminow, I.P., and Carruthers, J.R.: 'Optical waveguiding layer in $LiNbO_3$ and $LiTaO_3$', *Appl. Phys. Lett.*, vol. 13, pp. 2333-2342, 1974

7.2 Karge, H., Gotz, G., Jahn, U., and Schmidt, S.: 'Radiation damage and refractive index of ion-implanted $LiNbO_3$', *Nucl. Instr. and Methods*, vol. 182/183, pp. 777-780, 1981

7.3 Al-Chalabi, S.A.M.: 'Transient annealing of planar waveguides formed by He^{4+} ion implantation into $LiNbO_3$', *Solid-State Electron.*, vol. 30, pp. 227-231, 1987

7.4 Schmidt, R., and Kaminow, I.: 'Metal-diffused optical waveguides in $LiNbO_3$', *Appl. Phys. Lett.*, vol. 225, pp. 458-460, 19974

7.5 Jackel, J.L., and Rice, C.E.: 'Topotactic $LiNbO_3$ to cubic perovskite structural transformation in $LiNbO_3$ and $LiTaO_3$', *Ferroelectrics*, vol. 38, pp. 607-608, 1981

7.6 Jackel, J.L., Rice, C.E., and Veselka, J.J.: 'Proton exchange for high-index waveguides in $LiNbO_3$', *Appl. Phys. Lett.*, vol. 41, pp. 607-608, 1982

7.7 Suchoske, P.G., Findakly, T.K., and Leonberger, F.J.: 'Stable low-loss proton exchanged $LiNbO_3$ waveguide devices with no electro-optic degradation', *Optics Lett.*, vol. 13(11), pp. 1050-1052, 1988

7.8 Rice, C.E.: 'The structure and properties of $Li_{1-x}H_xNbO_3$', *J. Solid State Chem.*, vol. 64, pp. 188-199, 1986

7.9 Rice, C.E., and Jackel, J.: 'Structural changes with composition and temperature in rhombohedral $Li_{1-x}H_xNbO_3$', *Mater. Res. Bull.*, vol. 19, pp. 591-597, 1984

7.10 Minakata, M., Kumagai, K., and Kawakami, S.: 'Lattice constant changes and electro-optic effects in proton exchange $LiNbO_3$ optical waveguides', *Optoelectronics-Divisions and Technol.*, vol. 1(2), pp. 163-173, 1986

7.11 Clark, D.F., Nutt, A.C.G., Wong, K.K., Laybourn, P.J.R., and De La Rue, R.M.: 'Characterization of proton exchange slab optical waveguides in z-cut $LiNbO_3$', *J. Appl. Pyhs.*, vol. 54, pp. 6218-6220, 1983

8.0 PERSONNEL

The Principal Investigator for this program is Professor William B. Bridges, who was directly involved in all phases of the work.

Dr. Finbar T. Sheehy was the senior Graduate Research Assistant on this project and was involved in all phases of antenna coupled modulators from their inception in 1989 through June 1993, when he received his Ph. D. in Electrical Engineering from Caltech. Much of the material in his doctoral dissertation is contained in this final report. Dr. Sheehy now works for McKinsey and Company in Los Angeles.

Mr. Lee J. Burrows received his B. S. in Applied Physics from Caltech in June 1992, and joined the project that same month. He received his M. S. in Applied physics in June 1993, and is now in his third year of graduate studies in Applied Physics; he is now the senior Graduate Research Assistant on this project. Mr. Burrows has taken up the demonstration of Sheehy's idea for the Slot-V antenna-coupled modulator (Section 6 of this report), and also has undertaken the study of proton-exchange waveguides (Section 7 of this report)

Mr. Uri V. Cummings worked on this project during the summer of 1993 under Caltech's Summer Undergraduate Research Fellowship (SURF) program. Mr. Cummings took up the work begun by Dr. Sheehy on the mm-wave directional coupler modulator, described in Sec. 3 of this report and then continued the work as his Senior Thesis project. He received his B. S. in Electrical Engineering from Caltech in June 1994, and joined our research group as a graduate student and continues to work on DCM's. He received his M. S. in Electrical Engineering in June 1995.

Mr. Aaron W. Rempel worked on this project under Caltech's SURF program during the summer of 1993. He contributed to the first proton exchange waveguide fabrication and to the initial tests of our crystal polishing facility. He Received his B. S. in Applied Physics from Caltech in June 1994 and is currently a first year graduate student at U.S.C. in Electrical Engineering.

Mr. Reynold E. Johnson has contributed to the project as Staff Engineer on a part time basis since its inception. He has been with the research group since 1988, when he retired (early) from the Hughes Aircraft Company, Missle Group.

Dr. Axel Scherer, Professor of Electrical Engineering at Caltech, has been of invaluable assistance in helping us to setup our modulator and waveguide fabrication capability, and in our attempts at understanding the physical structure of lithium niobate. He has allowed us generous use of his time and equipment.

Dr. James H. Schaffner at the Hughes Research Laboratories has continued his informal collaboration with this project, fabricating all of the modulators to date and many test samples for us.

9.0 INTERACTIONS, PAPERS, AND PATENTS

9.1 MEETINGS AND CONFERENCES

Mr. Norman P. Bernstein attended briefings at Hughes Research Labs (with Brian Hendrickson) on 8 June, and at Caltech on 29 November 1992, 10 June and 17 December 1993, 24 June 1994 and 13 June 1995 for briefings on project progress.

The following conferences and meetings were attended by project personnel:

(Bridges) Government Microcircuit Applications Conference (GOMAC), Orlando FL, 5-7 November 1991. Paper 13.3, "Velocity-Matched External Modulator for EHF Transmission."

(Bridges) Photonics Systems for Antenna Applications (PSAA-II), Monterey CA, 10-12 December 1991. Paper, "Wave-Coupled W-Band $LiNbO_3$ Mach-Zehnder Modulator."

(Bridges) visited N. P. Bernstein at Rome Laboratories, NY, July 1992.

(Bridges) Joint Meeting of IEEE Antennas and Propagation Society, URSI, and Nuclear EMP, Chicago, IL, 18-25 July 1992. Paper , "Wave-Coupled W-Band $LiNbO_3$ Mach-Zehnder Modulator."

(Bridges, Burrows) IEEE/LEOS summer conference on Broadband Analog Fiber Optic Communications,Santa Barbara CA, July 1993.

(Bridges) PSAA-IV, Monterey CA, 18-21 January 1994, Paper, "Wave-Coupled $LiNbO_3$ Directional Coupler Modulator at 94 GHz."

(Bridges) DoD Fiber Optics Conference, 22-24 March 1994. Paper: "Progress in Antenna-Coupled Millimeter-Wave Electro-Optic Modulators."

(Bridges) Rome/AFOSR Review, Rome Laboratories, NY, 2 June 1994. Paper: "Review of Antenna Coupled Modulators for mm-Waves."

(Bridges) Lincoln Laboratories, Lexington MA, 3 June 1994. Paper "Review of Antenna Coupled Modulators for mm-Waves, and Linearized Fiber Optic Analog R-F Links."

(Bridges) PSAA-V, Monterey CA, January 18-20, 1995.

(Bridges) IEEE/LEOS summer conference, Keystone CO, August 1995. Paper (invited) "Review of Linearized Analog Fiber Optic Links."

9.2 PUBLICATIONS

J. H. Schaffner and W. B. Bridges, "Intermodulation Distortion in High Dynamic Range Microwave Fiber Optic Links with Linearized Modulators," IEEE J. Lightwave Tech., vol. 5, pp. 307-310, March 1993.

F. T. Sheehy, W. B. Bridges and J. H. Schaffner, "94 GHz Antenna-Coupled $LiNbO_3$ Electro-Optic Modulators," IEEE Photonics Technology Letters, vol. 5, pp 307-310, March 1993.

F. T. Sheehy, "Antenna-Coupled mm-Wave Electro-Optic Modulators and Linearized Electro-Optic Modulators," Ph. D. Dissertation, California Institute of Technology, June 1993.

W. B. Bridges and J. H. Schaffner, "Distortion in Linearized Electro-Optic Modulators," IEEE Trans. on Microwave Theory and Tech., vol. 43, pp. 2184-2197, September 1995.

9.3 PATENTS

U. S. Patent 5,309,531, based on work done prior to the present contract on the Slot-V antenna-coupled modulator, issued to F. T. Sheehy on May 3, 1994.

GLOSSARY

Align-Rite A commercial photolithographic mask maker in Burbank CA.

a_h Length of the hexagonal unit cell.

Band designations:

X-Band: The frequency range 8.2 to 12.4 GHz

K-Band: The frequency range 18 to 26.5 GHz

V-Band: The frequency range 50 to 75 GHz

W-Band: The frequency range 75 to 110 GHz

c_h Height of a hexagonal unit cell.

DCM Directional Coupler Modulator.

FTS-1 Antenna-coupled directional coupler modulator for 94 GHz designed by Finbar T. Sheehy.

H-plane antenna: The antenna pattern in the plane of symmetry where the magnetic fields (H) lie in the plane and the electric fields (E) are everywhere normal to it.

HRL Hughes Research Laboratories

L_0 Cross-over length in a directional coupler. The propagation distance for all of the power in one arm to transfer to the other arm

$LiNbO_3$: Lithium Niobate; a transparent crystalline material which displays a strong electro-optic effect.

LINC-1 Designation of a particular waveguide mask designed by Hughes Research Labs.

LJB-el- Electrode masks designed by Lee J. Burrows, numbered sequentially.

LJB-wg- Wave guide masks designed by Lee J. Burrows, numbered sequentially.

m Modulation fraction in amplitude modulation.

mm-wave: Millimeter-wave; the frequency range 30 to 300 GHz. Often the word "microwave" is intended to include all or part of the millimeter-wave range.

MZ Mach-Zehnder; a form of two-beam interferometer.

MZM Mach-Zehnder electro-optic amplitude modulator. Achieved by splitting the input optical beam into two paths, phase-modulating the paths separately, and then recombining the paths into one beam. If the phase-difference between the paths is zero, the output intensity will be a maximum. If the phase-difference is 180°, the output intensity will be zero (or a minimum).

n Optical refractive index; the ratio of the speed of light in a vacuum to the speed of the signal in the material.

$\mathbf{n_{neff}}$ Effective value of n for a transmission line on a dielectric interface.

PSAA- Photonic Systems for Antenna Applications conference; numbered sequentially.

$\mathbf{r_{33}}$ Electro-optic coefficient

Sinc Abbreviation for the sin(x)/x function.

Slot V Antenna The dual of the V Antenna, where conductor is replaced aperture in a metal ground plane.

Stycast® Trademark for artificial dielectric material made by Emerson and Cummins.

SURF Summer Undergraduate Research Fellowship (at Caltech).

UTP Uniphase Telecommunications Products (formerly United Technology Photonics).

UVC-el- Electrode masks designed by Uri V. Cummings; numbered sequentially.

UVC-wg- Waveguide masks designed by Uri V. Cummings; numbered sequentially.

V Antenna Dipole antenna with dipole arms forming an angle less than 180°. Usually the dipole arms are several wavelengths long.

V_π Half-wave voltage for a Mach-Zehnder modulator. The voltage change required to turn the modulator from fully off to fully on.

V_S Voltage required to shift the optical signal from one arm to the other in a directional coupler modulator.

WR- Electronics Industry Association designation for standard waveguide

WR-10	0.050" x 0.100"	75 - 110 GHz	W-Band
WR-15	0.075" x 0.150"	50 - 75 GHz	V-Band
WR-42	0.170" x 0.420"	18 - 26.5 GHz	K-Band
WR-90	0.400" x 0.900"	8.2 - 12.4 GHz	X-Band

x Atomic fraction of an element in a crystal.

α Designation for the phase in the lithium- hydrogen niobate system that occurs for the smallest value of hydrogen fraction x.

$\beta, \beta', \beta'', \beta'''...\gamma$ Designations for phases in the lithium-hydrogen niobate system that occur for increasing values of the hydrogen fraction x..

β Optical propagation phase constant for a wave in an waveguide.

β_1, β_2 Optical propagation phase constants for the two waveguides in a directional coupler.

$\Delta\beta_e$ Change in the difference $\beta_1 - \beta_2$ induced by an applied electric field.

$\Delta\beta_S$ Static difference $\beta_1 - \beta_2$ resulting from non identical fabrication of two coupled waveguides.

Δa_h Change in hexagonal unit cell length.

Δc_h Change in hexagonal unit cell height.

Δn_e Change in the extra-ordinary index of refraction of a crystal.

Δn_o Change in the ordinary index of refraction of a crystal.

ε Relative permittivity for a dielectric; the dielectric constant.

λ Wavelength. in free space

λ_g Guide wavelength.

Appendix A

Radiation Pattern of the Interfacial Antenna

A1. Introduction

The problem of an antenna on a dielectric half-space (or at the interface between two dielectric half-spaces) has been addressed by a number of workers [1 - 4] using a variety of mathematical techniques. In particular [3] is quite detailed. The purpose of this appendix is to provide physical insight into the mechanisms which affect the antenna pattern of an interfacial antenna, and to use this insight to show explicitly how the antenna pattern of an interfacial wire antenna of arbitrary length and shape can be computed. By way of illustration, the radiation pattern of a thin V-antenna of arbitrary length and angle is computed in closed form, subject to the assumption that the current distribution in the wire is sinusoidal. Special cases of interest include the infinitesimal interfacial dipole, which has been analysed previously by Engheta et al. [2] by a method which is more mathematically involved than that presented here. This method gives an identical result.

A2. The Interfacial Antenna

Consider an antenna above a dielectric interface. Suppose the antenna lies entirely in a plane parallel to the interface, so that its antenna pattern above that plane is a mirror image of its pattern below it (in the absence of the interface itself). Referring to Figure A1, the far-field of the antenna in the direction (θ) in the presence of the interface is composed of two parts: one is

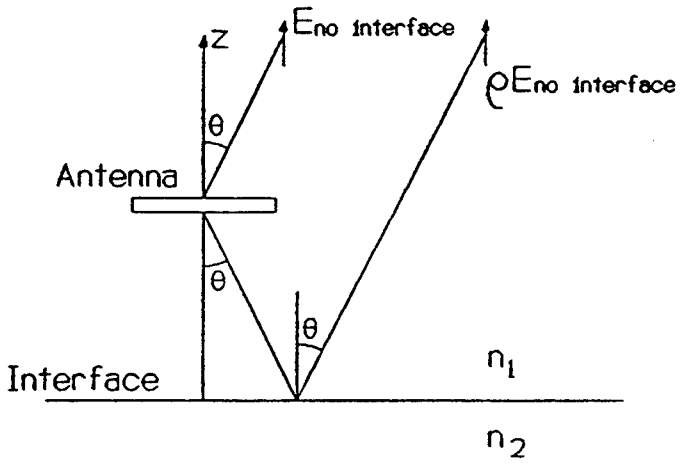

Figure A1 Computation of Antenna Pattern of an Antenna Above a Dielectric Interface

the direct radiation in that direction by the antenna in the absence of the interface; the other is the radiation reflected by the dielectric interface. Note that only the antenna far-fields need be considered, even though the dielectric interface itself may be in the near-field - this point is addressed in [3]. Essentially, fields which are not radiated by the antenna are not radiated after reflection from a surface which is invariant in the plane of reflection. The problem of finding the far-field of the antenna can be solved by linear superposition of radiation fields from the antenna itself and from its reflection in the dielectric interface. The reflected wave is the same as the direct wave except for a phase term due to the extra distance traveled and a reflection coefficient which in general affects both amplitude and phase. As the antenna moves closer to the interface the phase term due to extra distance traveled becomes smaller. When the antenna lies on the interface this phase term disappears entirely, and the far-field in the medium n_1 is simply

$$E_{far} = E_{no\ interface} (1 + \rho) . \tag{1}$$

The reflection coefficient ρ depends on both the angle of incidence and polarization of the wave. For horizontally polarized waves it is :

$$\rho = \frac{n_1 \cos\theta_1 - n_2 \cos\theta_2}{n_1 \cos\theta_1 + n_2 \cos\theta_2} , \tag{2}$$

where θ_1 is the angle of incidence,

and $$\cos\theta_2 = \sqrt{1 - \left(\frac{n_1}{n_2}\right)^2 \sin^2\theta_1} . \tag{3}$$

For vertically polarized waves the reflection coefficient is:

$$\rho = \frac{n_1 \cos\theta_2 - n_2 \cos\theta_1}{n_1 \cos\theta_2 + n_2 \cos\theta_1} . \tag{4}$$

Using the co-ordinate system in Figure A2, the waves transmitted by the antenna may be analysed into two components, whose electric field vectors are $E_\theta(r,\theta,\phi)$ and $E_\phi(r,\theta,\phi)$. At the dielectric interface these components are, respectively, vertically and horizontally polarized. If the field components transmitted by the antenna in the absence of an interface in the direction (r,θ,ϕ) are denoted as $E_{i\theta}(r,\theta,\phi)$ and $E_{i\phi}(r,\theta,\phi)$, then the following expressions hold:

$$E_\theta(r,\theta_1,\phi) = E_{i\theta}(r,\theta_1,\phi)\left(1 + \frac{n_1 \cos\theta_2 - n_2 \cos\theta_1}{n_1 \cos\theta_2 + n_2 \cos\theta_1}\right), \tag{5}$$

$$E_\phi(r,\theta_1,\phi) = E_{i\phi}(r,\theta_1,\phi)\left(1 + \frac{n_1 \cos\theta_1 - n_2 \cos\theta_2}{n_1 \cos\theta_1 + n_2 \cos\theta_2}\right). \tag{6}$$

Rewriting these in terms of θ_1 only, and writing θ_1 as θ now,

$$E_\theta(r,\theta,\phi) = E_{i\theta}(r,\theta,\phi)\,\frac{2\,n_1\sqrt{1 - \left(\frac{n_1}{n_2}\right)^2 \sin^2\theta}}{n_2 \cos\theta + n_1\sqrt{1 - \left(\frac{n_1}{n_2}\right)^2 \sin^2\theta}}, \tag{7}$$

$$E_\phi(r,\theta,\phi) = E_{i\phi}(r,\theta,\phi)\,\frac{2\,n_1 \cos\theta}{n_1 \cos\theta + n_2\sqrt{1 - \left(\frac{n_1}{n_2}\right)^2 \sin^2\theta}} . \tag{8}$$

This reduces the problem of finding the antenna pattern of an antenna lying on a dielectric interface to one of finding the antenna pattern of the same antenna

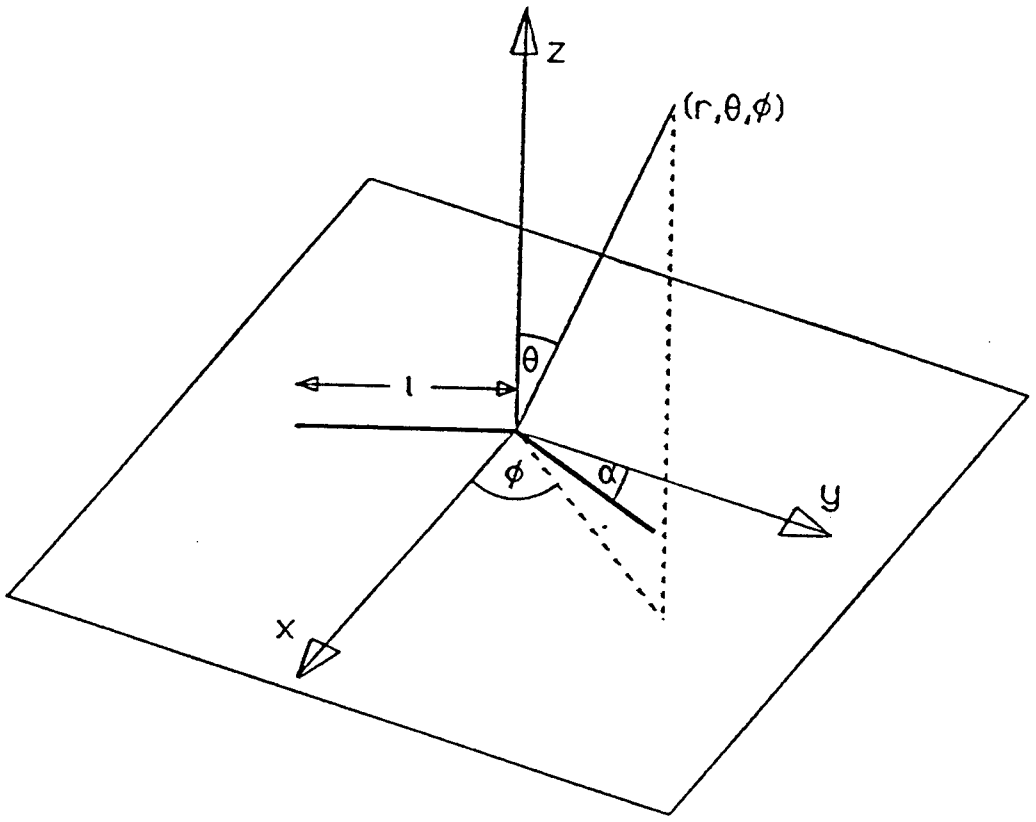

Figure A2 Co-ordinate System for the Antenna Pattern Computations

with the same current distribution in the absence of the interface (i.e., in dielectric n_1 only).

Up to this point we have not considered the effect of the interface on the near fields. The interface changes the current distribution on the antenna as a result of this interaction. For a thin wire antenna the current is distributed on the antenna as it would be if the antenna were embedded in a medium whose dielectric constant were between the values actually present on either side of the interface. This means that, although the problem has now been reduced to one in a single dielectric medium, it involves a current distribution which might not naturally exist in that medium. This means that deriving the pattern of an antenna on an interface from the measured pattern of one in a single medium is not possible in general, unless there is some way to force an appropriate current-distribution on the test antenna.

A3. Computation of $E_{i\theta}(\theta,\phi)$ and $E_{i\phi}(\theta,\phi)$ for a V-Antenna

The antenna pattern in the absence of an interface is computed using the magnetic vector potential function **A** [5], where

$$A(x,y,z,t) = \frac{e^{j(\omega t - kr)}\mu_o}{4\,\pi\,r} \int_V J(\xi,\eta)\, e^{jkL}\, dV\,, \tag{9}$$

in which
$$L = \xi \sin\theta \cos\phi + \eta \sin\theta \sin\phi\,, \tag{10}$$

where the (ξ,η) plane is the plane in which the antenna lies.

The magnetic vector potential **A** is the product of a spherical wave with the directional weighting function

$$\mathbf{a}(\theta,\phi) = \int_V \mathbf{J}(\xi,\eta)\, e^{jkL}\, d\xi\, d\eta\,. \tag{11}$$

Then:

$$\mathbf{E} = (c^2/j\omega)\ \nabla \times \nabla \times \mathbf{A}\,, \tag{12}$$

$$\mathbf{B} = \nabla \times \mathbf{A}\,. \tag{13}$$

Performing these operations, the result is that the radiated fields are:

$$\mathbf{E} = -j\omega \mathbf{A}_T\,, \tag{14}$$

$$\mathbf{H} = \left(\frac{1}{\eta}\right) \mathbf{1}_r \times \mathbf{E}\,, \tag{15}$$

and the average power density at the point (r,θ,ϕ) is given by:

$$P(r,\theta,\phi) = \frac{1}{2}\left(\frac{k_1^{\,2}\,\eta_1}{(4\,\pi\,r)^2}\right)\left(\,|\,a_\theta(\theta,\phi)\,|^2 + |\,a_\phi(\theta,\phi)\,|^2\,\right). \tag{16}$$

The V-antenna is in two parts, which may be parameterized as follows:

<u>Part 1</u> Parameter q : $-\ell < q < 0$

$$\left.\begin{aligned} &I_\xi(q) = -\ I_o \sin\alpha \sin[k_a\,(\ell + q)\,] \\ &I_\eta(q) = I_o \cos\alpha \sin[k_a\,(\ell + q)\,] \\ &\text{Phase Parameter } L = q \sin\theta \sin(\phi - \alpha)\,; \end{aligned}\right\} \tag{17}$$

Part 2 Parameter q: $0 < q < \ell$

$$\left.\begin{aligned} I_\xi(q) &= I_o \sin\alpha \sin[k_a (\ell - q)] \\ I_\eta(q) &= I_o \cos\alpha \sin[k_a (\ell - q)] \end{aligned}\right\} \quad (18)$$

Phase Parameter $L = q \sin\theta \sin(\phi+\alpha)$.

Notice that the current distribution in each part is sinusoidal, with wavelength $\lambda_a = \frac{2\pi}{k_a}$. This wavelength depends on the presence of the interface, although the rest of the calculation does not take the existence of the interface into account at all (remember, this calculation is to find the antenna pattern in the absence of the interface). The determination of the constant k_a is not actually necessary for the mathematics, although obviously it must be determined before the resulting antenna pattern can be computed. Kominami et al. [4] have determined that, for infinitesimal dipole thickness, k_a is given by:

$$k_a = \sqrt{\frac{k_1^2 + k_2^2}{2}} , \quad (19)$$

where k_1 and k_2 are the wavenumbers in the two dielectrics.

The component $a_{i\theta}(\theta,\phi)$ is given by [5]

$$a_{i\theta}(\theta,\phi) = I_o \cos\theta \int_{-\ell}^{0} \sin[k_a(\ell + q)] \sin(\phi - \alpha)\, e^{j\, k\, q \sin\theta \sin(\phi-\alpha)}\, dq ,$$

$$+I_o \cos\theta \int_{0}^{\ell} \sin[k_a(\ell - q)] \sin(\phi+\alpha)\, e^{j\, k\, q \sin\theta \sin(\phi+\alpha)}\, dq . \quad (20)$$

In order to evaluate this integral, it is useful to know that

$$\int e^{ax} \sin(bx + c)\, dx = \frac{e^{ax}}{a^2 + b^2} [\, a \sin(bx + c) - b \cos(bx + c)\,] .$$

(21)

The full result is:

$$a_{i\theta}(\theta,\phi) = \cos\theta \sin(\phi-\alpha) \frac{k_a[\cos\{k\ell \sin\theta \sin(\phi-\alpha)\} - \cos(k_a\ell)]}{k_a{}^2 - k^2 \sin^2\theta \sin^2(\phi-\alpha)}$$

$$+ \cos\theta \sin(\phi+\alpha) \frac{k_a[\cos\{k\ell \sin\theta \sin(\phi+\alpha)\} - \cos(k_a\ell)]}{k_a{}^2 - k^2 \sin^2\theta \sin^2(\phi+\alpha)}$$

$$+ j \cos\theta \sin(\phi-\alpha) \frac{k \sin\theta \sin(\phi-\alpha) \sin(k_a\ell) - k_a \sin\{k\ell \sin\theta \sin(\phi-\alpha)\}}{k_a{}^2 - k^2 \sin^2\theta \sin^2(\phi-\alpha)}$$

$$+ j \cos\theta \sin(\phi+\alpha) \frac{-k \sin\theta \sin(\phi+\alpha) \sin(k_a\ell) + k_a \sin\{k\ell \sin\theta \sin(\phi+\alpha)\}}{k_a{}^2 - k^2 \sin^2\theta \sin^2(\phi+\alpha)} .$$

(22)

The ϕ-component comes from the integral

$$a_{i\phi}(\theta,\phi) = \int_{-\ell}^{0} \sin[k_a(\ell+q)] \cos(\phi-\alpha)\, e^{j\, k\, q \sin\theta \sin(\phi-\alpha)}\, dq$$

$$+ \int_{0}^{\ell} \sin[k_a(\ell-q)] \cos(\phi+\alpha)\, e^{j\, k\, q \sin\theta \sin(\phi+\alpha)}\, dq .$$

(23)

The closed-form solution of this integral is:

$$a_{i\phi}(\theta,\phi) = \cos(\phi-\alpha) \frac{k_a[\cos\{k\ell \sin\theta \sin(\phi-\alpha)\} - \cos(k_a\ell)]}{k_a{}^2 - k^2 \sin^2\theta \sin^2(\phi-\alpha)}$$

$$+ \cos(\phi+\alpha)\,\frac{k_a[\cos\{k\ell\,\sin\theta\,\sin(\phi+\alpha)\}-\cos(k_a\ell)]}{{k_a}^2-k^2\,\sin^2\theta\,\sin^2(\phi+\alpha)}$$

$$+ j\,\cos(\phi-\alpha)\,\frac{k\,\sin\theta\,\sin(\phi-\alpha)\,\sin(k_a\ell)-k_a\,\sin\{k\ell\,\sin\theta\,\sin(\phi-\alpha)\}}{{k_a}^2-k^2\,\sin^2\theta\,\sin^2(\phi-\alpha)}$$

$$+ j\,\cos(\phi+\alpha)\,\frac{-k\,\sin\theta\,\sin(\phi+\alpha)\,\sin(k_a\ell)+k_a\,\sin\{k\ell\,\sin\theta\,\sin(\phi+\alpha)\}}{{k_a}^2-k^2\,\sin^2\theta\,\sin^2(\phi+\alpha)}\,. \tag{24}$$

The complete result for power density at a point (r,θ,ϕ) in dielectric n_1 for the V-antenna, when the effect of the interface on each of the field components is included, is:

$$P(r,\theta,\phi)=\frac{{I_o}^2}{2}\left(\frac{{k_1}^2\,\eta_1}{(4\,\pi\,r)^2}\right)\left(|\,a_{i\theta}(\theta,\phi)\,|^2\,\frac{4\,{n_1}^2\left(1-\left(\frac{n_1}{n_2}\right)^2\sin^2\theta\right)}{\left|\,n_2\cos\theta+n_1\sqrt{1-\left(\frac{n_1}{n_2}\right)^2\sin^2\theta}\,\right|^2}\right.$$

$$\left.+\,|\,a_{i\phi}(\theta,\phi)\,|^2\,\frac{4\,{n_1}^2\cos^2\theta}{\left|\,n_1\cos\theta+n_2\sqrt{1-\left(\frac{n_1}{n_2}\right)^2\sin^2\theta}\,\right|^2}\right), \tag{25}$$

where $a_{i\theta}(\theta,\phi)$ and $a_{i\phi}(\theta,\phi)$ are given in equations (22) and (24) respectively.

A4. Special Case: Dipole in Free Space

As a "sanity-check" on these results, we can compare the above with some known results in special cases, the simplest of which is the straight dipole in free space. In this situation, the conditions applied to the above result are:

$$\left.\begin{aligned}&\alpha=0\\&k_1=k_a=k\\&n_1=n_2\,.\end{aligned}\right\} \tag{26}$$

Note that whenever α=0 the expression for radiated power simplifies considerably, as the imaginary terms cancel, and the real terms become equal to each other in pairs.

Then the result becomes:

$$P(r,\theta,\phi) = \frac{{I_o}^2\, n_1}{8\,\pi^2\, r^2}\sqrt{\frac{\mu_o}{\epsilon_o}}\;\frac{[\cos(k\ell\,\sin\theta\,\sin\phi) - \cos(k\ell)]^2}{\{1 - \sin^2\theta\,\sin^2\phi\}^2}\left(\cos^2\theta\,\sin^2\phi + \cos^2\phi\right). \tag{27}$$

This is indeed the expression for the antenna pattern of a dipole in free space. The total length of the dipole is 2ℓ.

A5. Special Case: V-Antenna in Free Space

Here the conditions are:

$$\left.\begin{aligned} k_1 &= k_a = k \\ n_1 &= n_2\,. \end{aligned}\right\} \tag{28}$$

The equations become a little simpler, but not much. Figure A3 shows the E-plane power pattern (i.e., in the plane of the antenna) for a V-antenna whose arms are each one wavelength long, and where the angle between the arms is 110°. This example is given by Carter et al. [6]. If the arms are made 8 wavelengths long, and the angle between them is decreased to 35°, we get a very directional pattern. The forward half of the E-plane pattern is shown in Figure A4. Note that the pattern is exactly the same in the other direction. This pattern can also be compared with [6].

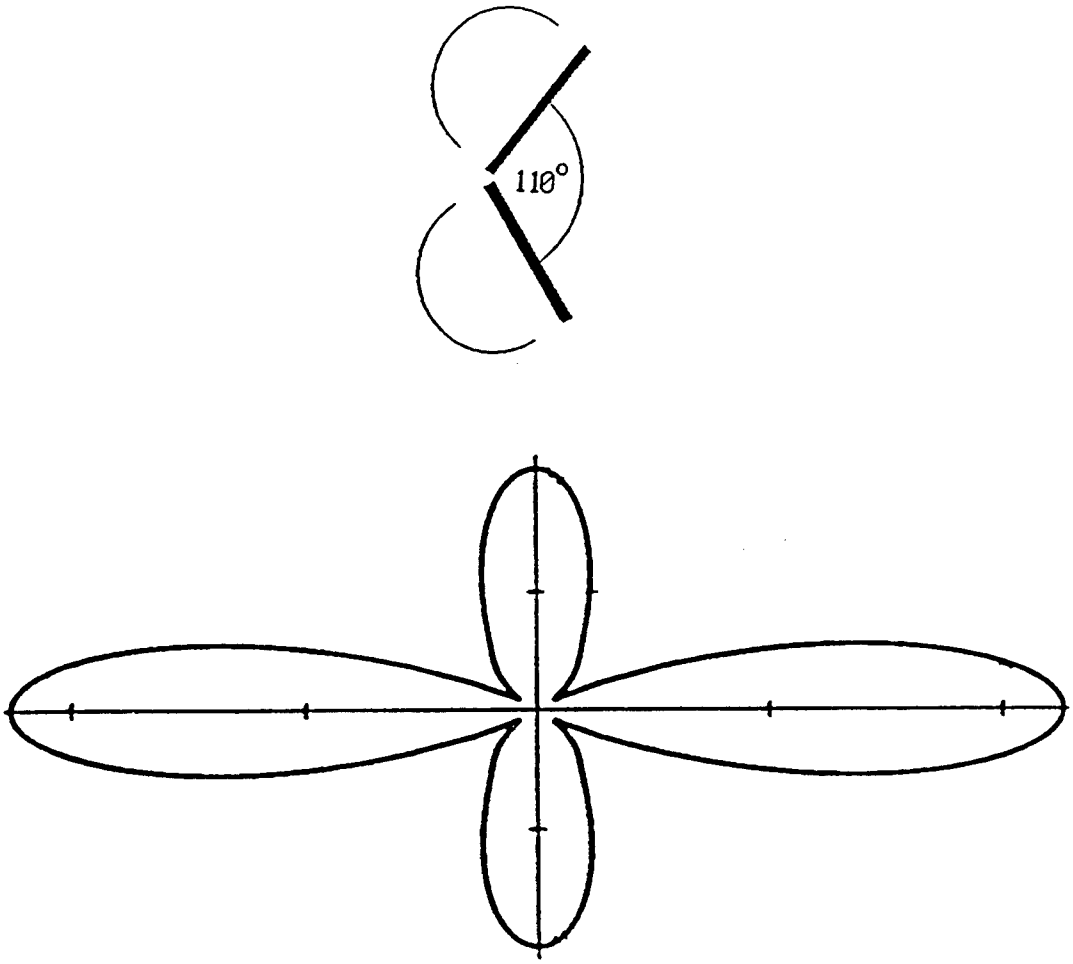

Figure A3 Antenna pattern of a V-antenna whose arms are each one wavelength long. The V-angle is 110°. The pattern shown is in the plane of the V (the E-plane).

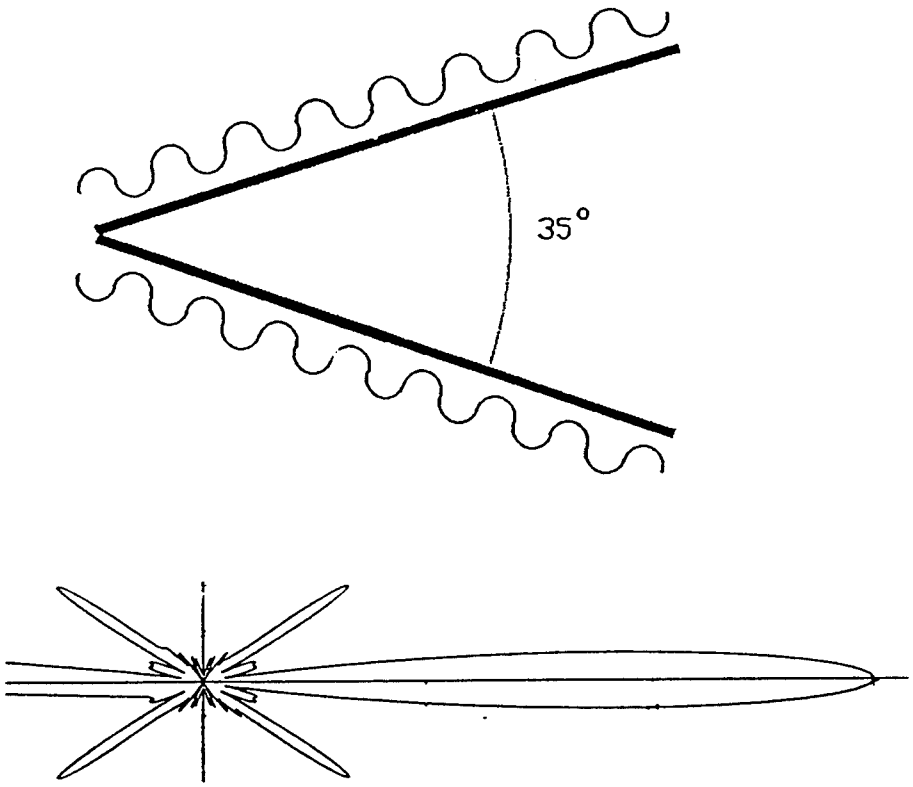

Figure A4 Antenna pattern of a V-antenna whose arms are each eight (8) wavelengths long. The V-angle is 35°. The pattern shown is in the plane of the V (the E-plane).

A6. Special Case: Infinitesimal Dipole on a Dielectric Half-Space

This time the conditions are:

$$\left.\begin{aligned} \alpha &= 0 \\ k_1 &= k \\ n_1 &= n \\ n_2 &= 1 \\ \ell &\to 0 \,. \end{aligned}\right\} \quad (29)$$

Now the expression for radiated power becomes:

$$P(r,\theta,\phi) = \lim_{\ell \to 0} \frac{I_o^2 k^2 n^3}{2 \pi^2 r^2} \sqrt{\frac{\mu_o}{\epsilon_o}} \cos^2\theta \, \frac{\left(\cos(k\ell \sin\theta \sin\phi) - \cos(k_a \ell)\right)^2}{k_a^2 \left(1 - \left(\frac{k}{k_a}\right)^2 \sin^2\theta \sin^2\phi\right)^2}$$

$$x \left(\frac{|1 - n^2 \sin^2\theta| \ \sin^2\phi}{|\cos\theta + n\sqrt{1 - n^2 \sin^2\theta}\,|^2} + \frac{\cos^2\phi}{|n\cos\theta + \sqrt{1 - n^2 \sin^2\theta}\,|^2} \right). \quad (30)$$

Expanding the cosine terms which involve ℓ as power series,

$$P(r,\theta,\phi) = \lim_{\ell \to 0} \frac{I_o^2 k^2 k_a^2 n^3 \ell^4}{8 \pi^2 r^2} \sqrt{\frac{\mu_o}{\epsilon_o}} \cos^2\theta \left(\frac{|1 - n^2 \sin^2\theta|}{|\cos\theta + n\sqrt{1 - n^2 \sin^2\theta}\,|^2} \sin^2\phi \right.$$

$$\left. + \frac{\cos^2\phi}{|n\cos\theta + \sqrt{1 - n^2 \sin^2\theta}\,|^2} \right). \quad (31)$$

The input current to the dipole is $I_o \sin(k_a \ell)$, which becomes $I = I_o k_a \ell$ as

$\ell \to 0$, so

$$P(r,\theta,\phi) = \frac{I^2 k^2 n^3 \ell^2}{8 \pi^2 r^2} \sqrt{\frac{\mu_o}{\epsilon_o}} \cos^2\theta \left(\frac{|1 - n^2 \sin^2\theta|}{|\cos\theta + n\sqrt{1 - n^2 \sin^2\theta}\,|^2} \sin^2\phi + \frac{\cos^2\phi}{|n\cos\theta + \sqrt{1 - n^2 \sin^2\theta}\,|^2} \right). \quad (32)$$

This expression is in a somewhat different form to that derived by Engheta et al. [2], but with the appropriate changes of co-ordinates it is algebraically identical to that result.

A7. V-Antenna on a Dielectric Half-Space

The most general case, the V-antenna on a dielectric half-space, requires the full set of equations (22), (24), and (25). For antennas whose arm-lengths are smaller than one-half interface wavelength long, bending the antenna into a V does not do anything very interesting. Figures A5 and A6, for example, show the H-plane patterns (i.e., in the plane, normal to the interface, which bisects the V) of a straight two-half-waves-in-phase dipole and a 140° two-half-waves-in-phase V, respectively, on a substrate of ϵ=28. There is very little difference between the two. On the other hand, if the arm-lengths are increased to one interface wavelength, there is no power transmitted in the H-plane by a straight dipole, but if the antenna is bent to form a 100° V, its H-plane pattern is as shown in Figure A7.

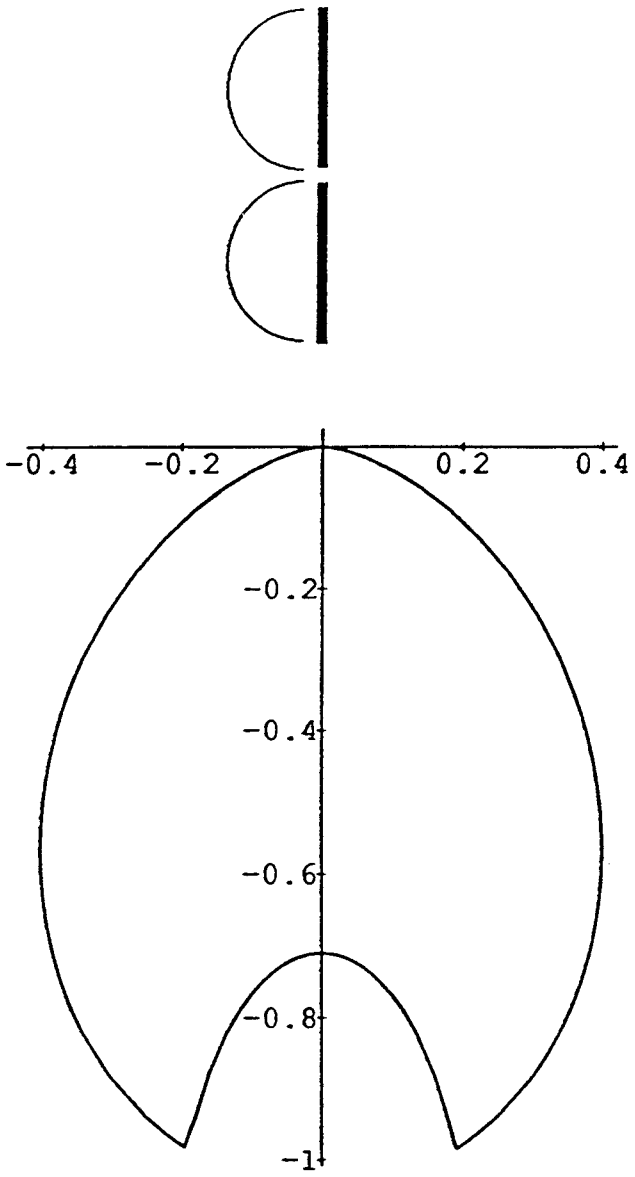

Figure A5 Antenna pattern of a two-half-waves-in-phase dipole on the surface of a dielectric, $\epsilon = 28$. The pattern shown is in the dielectric, in the plane normal to the dipole (the H-plane).

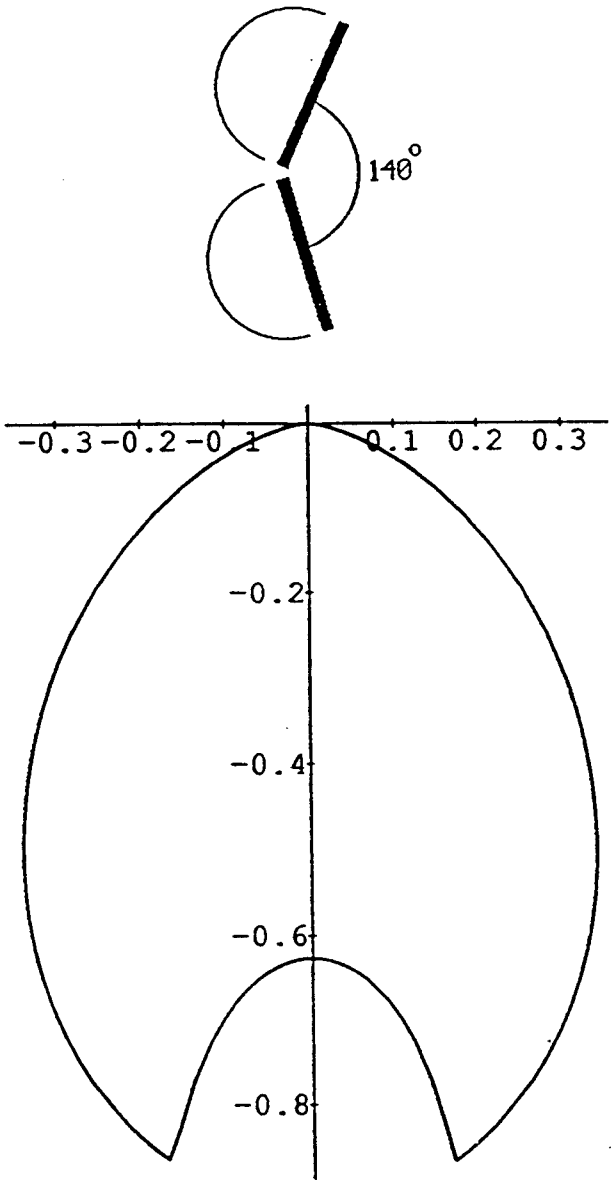

Figure A6 Antenna pattern of a V antenna on the surface of a dielectric, $\epsilon = 28$. Each arm of the V is one half-surface-wavelength long. The V angle is 140°. The pattern shown is in the dielectric, in the plane which bisects the V.

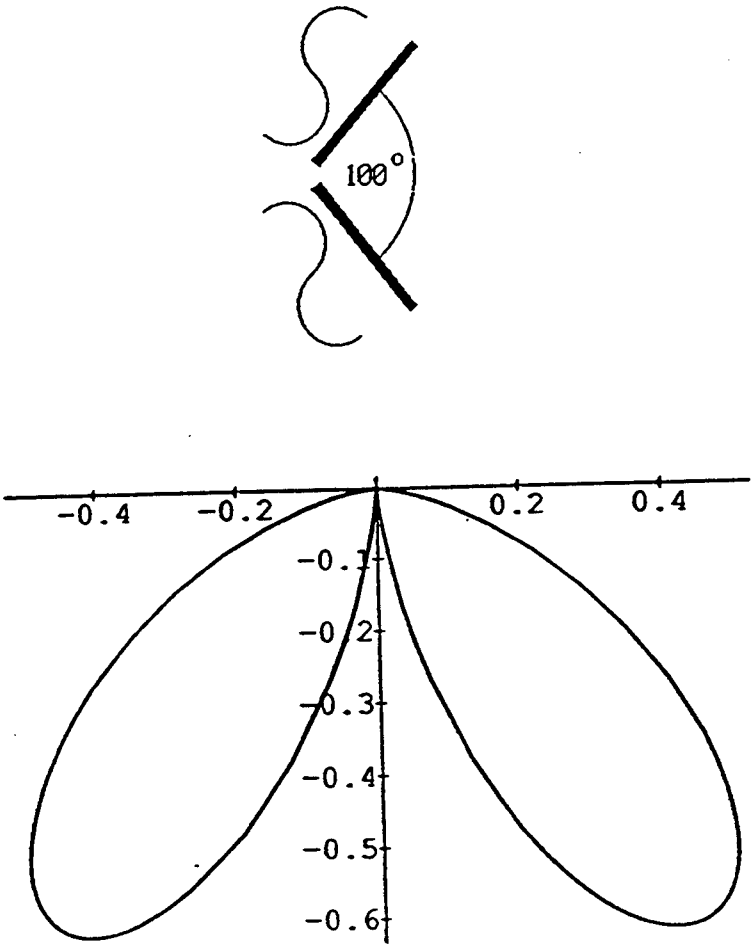

Figure A7 Antenna pattern of a V antenna on the surface of a dielectric, ϵ-28. Each arm of the V is one surface-wavelength long. The V angle is 100°. The pattern shown is in the dielectric, in the plane which bisects the V.

A8. Conclusion

I have shown a practical method of computing the complete far-zone fields and radiated power pattern of an arbitrarily-shaped wire antenna on the interface between two dielectric half-spaces, assuming known (e.g., sinusoidal) current distribution on the wire. Physical insight into the mechanisms involved in the antenna pattern is the basis of the method. By way of illustration, the antenna pattern of an interfacial V-antenna of arbitrary length and angle is computed, compared with known results in special cases, and used to show the behavior of some interfacial V-antennas.

References

[1] C. R. Brewitt-Taylor, D. J. Gunton and H. D. Rees, "Planar Antennas on a Dielectric Surface," Electron. Lett. Vol. 17, No. 20, 1^{st} October 1981

[2] N. Engheta, C.H. Papas and C. Elachi, "Radiation Patterns of Interfacial Dipole Antennas," Radio Science, Vol. 17, No. 6, pp. 1557-1566, November-December 1982

[3] G. S. Smith, "Directive Properties of Antennas for Transmission into a Material Half-Space," IEEE Trans. Ant. & Prop., Vol. AP-32, No. 3, March 1984

[4] M. Kominami, D. M. Pozar and D. H. Schaubert, "Dipole and Slot Elements and Arrays on Semi-Infinite Substrates," IEEE Trans. Ant. & Prop., Vol. AP-33, No. 6, June 1985

[5] R. S. Elliott, Antenna Theory and Design, Ch. 1, Prentice-Hall, Inc., 1981

[6] P.S. Carter, C.W. Hansell, and N.E. Lindenblad, "Development of Directive Transmitting Antennas by R.C.A. Communications Inc.," Proc. IRE, Vol. 19, pp. 1773 - 1842, October 1931

*U.S. GOVERNMENT PRINTING OFFICE: 1996-509-127-47061

MISSION OF ROME LABORATORY

Mission. The mission of Rome Laboratory is to advance the science and technologies of command, control, communications and intelligence and to transition them into systems to meet customer needs. To achieve this, Rome Lab:

a. Conducts vigorous research, development and test programs in all applicable technologies;

b. Transitions technology to current and future systems to improve operational capability, readiness, and supportability;

c. Provides a full range of technical support to Air Force Material Command product centers and other Air Force organizations;

d. Promotes transfer of technology to the private sector;

e. Maintains leading edge technological expertise in the areas of surveillance, communications, command and control, intelligence, reliability science, electro-magnetic technology, photonics, signal processing, and computational science.

The thrust areas of technical competence include: Surveillance, Communications, Command and Control, Intelligence, Signal Processing, Computer Science and Technology, Electromagnetic Technology, Photonics and Reliability Sciences.